Enabling Soft Frequency Reuse and Stienen's Cell Partition in Two-Tier Heterogeneous Networks: Cell Deployment and Coverage Analysis

Ziaul Haq Abbas, Muhammad Sajid Haroon, *Student Member, IEEE*, Fazal Muhammad, *Member, IEEE*, Ghulam Abbas, *Senior Member, IEEE*, and Frank Y. Li, *Senior Member, IEEE*

***Abstract*—Heterogeneous cellular networks (HetNets) are one of the key enabling technologies for fifth generation (5G) networks. In HetNets, the use of small base stations (SBSs) inside the coverage area of a macro base station (MBS) offers higher throughput and improved coverage. However, such multi-tier base station deployment introduces new challenges, e.g., (i) All users experience significant inter-cell interference (ICI) due to frequency reuse, (ii) SBS associated users experience severe MBS-interference due to higher MBS transmit power, and (iii) MBS coverage edge users receive lower signal-to-interference ratio (SIR) due to longer distances. To address the aforementioned challenges, this work proposes a framework, including a novel cell deployment strategy, which combines Stienen's model with soft frequency reuse (SFR) and the corresponding performance analysis. According to Stienen's cell based SBS deployment, SBSs are deployed in MBS coverage edge area to enhance downlink SIR. To further mitigate ICI and MBS-interference, SFR is employed along with Stienen's cell based SBS deployment. Based on stochastic geometry, we derive expressions for coverage probability with four different types of cell deployment and SFR employment combinations. Numerical results indicate that SFR-enabled Stienen's cell based SBS deployment leads to enhanced edge user coverage and, hence, improves network performance gain.**

***Index Terms*—Heterogeneous cellular networks, Poisson hole process, Poisson point process, soft frequency reuse, Stienen's model, Coverage probability.**

I. Introduction

A. Motivation

Ubiquitous coverage with improved data rate is one of the major goals of heterogeneous cellular networks (HetNets) [1], [2]. In HetNets, small base stations (SBSs) are deployed in the coverage area of a macro base station (MBS) to enhance network coverage and improve capacity [3]. In the literature, the distributions of MBSs, SBSs and users in HetNets are oftentimes regarded as following Poisson point processes (PPPs) due to their tractability and accuracy [4], [5]. However, such multi-tier and ultra-dense SBS deployment leads to degraded network performance gain [6]. Some of the prominent challenges are as follows: (i) severe inter-cell interference (ICI) due to frequency reuse [7], (ii) significant MBS-interference (MBS-I) as a result of high MBS transmit power [8], [9], and (iii) lower received signal-to-interference ratio (SIR) by network edge users due to longer distances [8], [10]. Additionally, in a uniform SBS deployment, higher SBS density leads to significant co-channels interference.

ICI and MBS-I significantly degrade the coverage performance of HetNets [11], [12]. In [8], an effective resource allocation scheme was introduced to reduce ICI and MBS-I providing improved network coverage. To combat interference, one category of schemes is based on fractional frequency reuse (FFR) [13], where the complete system bandwidth, F, is divided into small sub-bands to abate interference and, hence, improve SIR. However, FFR leads to lower spectral efficiency due to partitioning of F [13]. Another category of interference mitigation schemes is based on soft frequency reuse (SFR) [14], [15]. SFR is spectrally more efficient, as compared with FFR, because all the bandwidth is made available for each tier of base stations (BSs) [16], [17]. Therefore, this work considers SFR to mitigate ICI and MBS-I.

For cell distribution, Stienen's model has been widely regarded as an effective network deployment approach since it leads to substantial reduction in interference via smart SBS deployment [18], [19]. For any MBS, a Stienen's cell can be formed by constructing a disc whose radius is equal to half of the distance between the two closest MBSs [19]. Accordingly, an MBS coverage region is divided into two regions, i.e., Stienen's cell area and its complementary area [20]. Such a coverage area division allows us to use various deployment densities of BSs in these two regions. In this work, we employ therefore Stienen's cell based SBS deployment model, where SBSs are only employed in the outer coverage area of an MBS cell providing improved downlink (D_L) SIR [21].

More specifically, we develop a cell deployment strategy, where SBSs are distributed via SFR-enabled Stienen's model to enhance MBS edge users' coverage. Being an effective net-

This work was presented in part as [1].

Manuscript received June 6, 2020; revised Nov. 23, 2020.

Z. H. Abbas is with the Faculty of Electrical Engineering, GIK Institute of Engineering Sciences and Technology, Topi 23640, Pakistan (email: ziaul.h.abbas@giki.edu.pk).

M. S. Haroon is with the Telecommunications and Networking (TeleCoN) Research Lab, GIK Institute of Engineering Sciences and Technology, Topi 23640, Pakistan (email: sajid.haroon@giki.edu.pk).

F. Muhammad is with the Department of Electrical Engineering, City University of Science and Information Technology, Peshawar 25000, Pakistan (email: fazal.muhammad@cusit.edu.pk).

G. Abbas is with the Faculty of Computer Science and Engineering, GIK Institute of Engineering Sciences and Technology, Topi 23640, Pakistan (email: abbasg@giki.edu.pk).

F. Y. Li is with the Department of Information and Communication Technology, University of Agder (UiA), N-4898 Grimstad, Norway (email: frank.li@uia.no).

work deployment approach, we termed SFR-enabled Stienen's model as a cell deployment strategy, where the BSs are smartly distributed to reduce network interference [20], [22]. Furthermore, we compare the results of the proposed cell deployment strategy with the uniform SBS deployment model. By employing SFR, complete bandwidth is available to both MBS associated users (MBS-AUs) and SBS associated users (SBS-AUs). In general, the proposed strategy leads to improved MBS edge users' coverage and the performance gain varies with different SIR threshold levels. In the best case, we find that SFR-enabled Stienen's cell based SBS deployment leads to 49% D_L coverage performance improvement in contrast with the uniform SBS deployment at an SIR threshold of -15 dB. The SFR scheme alone leads to 25% D_L coverage improvement at an SIR threshold of -15 dB.

B. Related Work

In what follows, we classify the related work into three categories, i.e., multi-tier deployment, interference mitigation schemes, and non-uniform HetNets (Nu-HetNets).

In the multi-tier deployment category, [8], [9] proposed two schemes to partition the coverage region of MBS into two non-overlapping sub-regions, i.e., cell interior region and cell edge region, for tractable coverage analysis. Users located in cell interior region encounter severe interference due to close proximity to high power MBS. Moreover, users located in cell edge region experience reduced signal-to-interference-plus-noise ratio (SINR) due to their distant locations. Furthermore, SBSs in cell interior region observe reduced coverage area due to high transmit power of MBS [9].

In the interference mitigation schemes category, SFR in a multichannel model was investigated along with average user rate in [14]. Moreover, SFR parameters and optimal combinations of association bias were analyzed. The authors conclude that SFR leads to improved coverage as compared with FFR under different network scenarios. The work in [23] presented SFR and FFR analytical models while using spatial PPP. The results in [23] indicate that SFR leads to higher spectral efficiency as compared with FFR. Mathematical models for SFR and FFR with load balancing in HetNets were developed in [24]. The results in [24] indicate that FFR leads to higher rate coverage while SFR provides improved spectral efficiency.

In the Nu-HetNets category, the authors in [25] proposed SBS muting near MBS, whereas keeping them active in the MBS edge area. Their proposed network setup results in improved rate and coverage performance in contrast to uniform SBS deployment due to reduced MBS-I. The authors in [26] considered coverage-oriented SBS distribution in MBS coverage area. According to their proposed model, SBSs are switched on/off based on their distances from the MBS. Their proposed setup leads to lower SBSs' density and, thus, enhances the network in contrast to uniform SBS deployment. Moreover, the authors investigated the coverage and rate performance of their proposed setup in [27]. The analysis in [27] indicates improved user throughput and coverage. The work in [18] proposed Stienen's cell SBS deployment in MBS coverage region. Their proposed model leads to significant coverage improvement as compared with uniform HetNets.

In this paper, we present SFR-enabled Stienen's cell based SBS deployment to enhance MBS edge users coverage and reduce MBS-I.

C. Approach and Contributions

This paper presents a framework for BS deployment in two-tier HetNets including a cell deployment strategy with proactive interference management scheme, the corresponding coverage probability analysis, and a means for performance improvement. The work presented in this paper distinguishes from the state-of-the-art studies with respect to the following aspects.

- The work in [14], [23], [24] focused on SFR and FFR performance analysis without considering Stienen's cell based SBS deployment, whereas we introduce SFR-enabled Stienen's cell based SBS deployment;
- The work in [25]–[27] considered NU-HetNets, whereas we combine Stienen's cell based SBS deployment along with the SFR scheme;
- Although the work in [18] proposed Stienen's cell based SBS deployment, it lacks the employment of a proactive[1] interference mitigation mechanism. This point is addressed in this paper;
- The work in [1] took into account load balancing with SFR, it lacks however the use of an effective network deployment approach, such as Stienen's model. In contrast, this work employs SFR-enabled Stienen's model and significantly reduces network interference by mitigating ICI and MBS-I.

In brief, the novelty and main contributions of this paper are summarized as follows:

1) This work proposes a novel cell deployment strategy which combines Stienen's model with SFR. To do so, (i) an MBS coverage area is divided into two regions based on the Stienen's model, where an MBS is located at the center of Stienen's cell and multiple SBSs are deployed outside the Stienen's cell, (ii) for SBS deployment, we introduce a Poisson hole process (PHP) instead of PPP, and (iii) SFR is enabled for spectrum allocation among both MBS and SBSs.
2) We derive the coverage probability expressions for the following network scenarios: (i) uniform SBS deployment with SFR, (ii) uniform SBS deployment without SFR, (iii) Stienen's cell based deployment model with SFR, and (iv) Stienen's cell based deployment model without SFR. Moreover, analyses are carried out for a reference user (RU) located (i) inside Stienen's cell and (ii) outside Stienen's cell.
3) To improve MBS edge users' performance, fewer SBSs are deployed near to the MBS. Consequently, SFR-enabled Stienen's cell deployment leads to reduced MBS-I and ICI due to proactive interference mitigation.

In the remaining part of this paper, we first present the system model and provide necessary preliminaries in Sec. II.

[1]By proactive, it is meant that an interference mitigation means is taken before a certain level of performance degradation occurs.

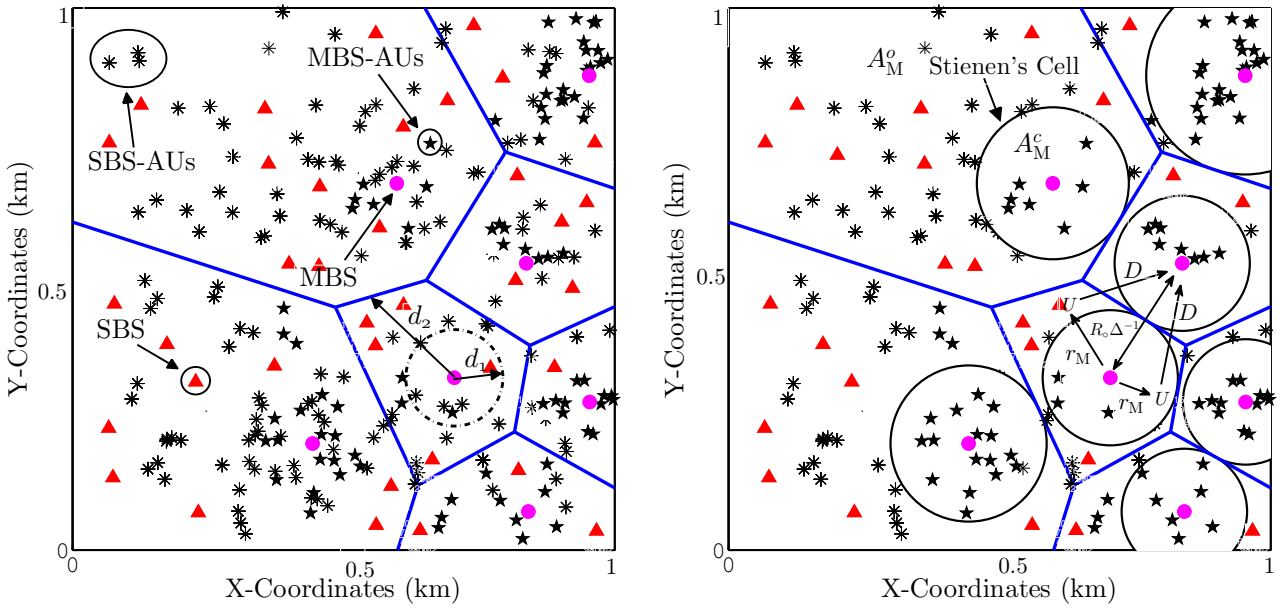

(a) Uniform SBS deployment model

(b) Stienen's cell based SBS deployment model

Fig. 1: Uniform HetNet model, where $\phi_{\nu,\mathrm{M}}$, $\phi_{\nu,\mathrm{S}}$, ϕ_{M}, and ϕ_{S}, are PPPs of MBS-AUs (pentagrams), SBS-AUs (asterisks), MBSs (dots), and SBSs (triangles), respectively, in Fig. 1a). Similarly, $\vec{\phi}_{\mathrm{S}}$ represents PHP of SBSs (triangles) in Fig. 1b).

TABLE I: Summary of major notations

Notation	Description
ϕ_{M} and ϕ_{S}	PPPs of MBSs and SBSs, respectively
$\phi_{\nu,\mathrm{M}}$ and $\phi_{\nu,\mathrm{S}}$	PPPs of MBS-AUs and SBS-AUs, respectively
$\vec{\phi}_{\mathrm{S}}$	PHPs of SBS
β_z	SIR threshold of zBS, $\forall\, z \in \{\mathrm{M}, \mathrm{S}\}$
λ_{M}, $\lambda_{\nu,\mathrm{M}}$	Densities of MBS and MBS-AUs, respectively, following PPP
λ_{S}, $\lambda_{\nu,\mathrm{S}}$	Densities of SBSs and SBS-AUs, respectively, following PPP
$\vec{\lambda}_{\mathrm{S}}$	Densities of SBSs following PHP
Δ	A constant, i.e., $\Delta = 1/2$
θ	Angle between $R_\circ\Delta^{-1}$ and r_{M}
r_j, r_k	User distances from jth and kth-tiers, $\forall\, j \in \{\phi_{\mathrm{M}}\}$ and $k \in \{\phi_{\mathrm{S}}\}$
RU	Reference user
$RU_{A^c_{\mathrm{M}}}$	$RU \in A^c_{\mathrm{M}}$
$RU_{A^o_{\mathrm{M}}}$	$RU \in A^o_{\mathrm{M}}$
r_{M}	Distance between MBS and RU
ψ	Ratio of r_{M} to $R_\circ$
$\lvert h\rvert$	Power gain of Rayleigh fading
F	Frequency band
ϱ	Stienen's cell deployment
ζ	Uniform SBS deployment
$*$	SFR employment

Afterwards, coverage probability expressions for the proposed setup are derived in Sec. III. Then, numerical and simulation results are presented in Sec. IV. Finally, we conclude the paper in Sec. V. In addition, a list of major notations used in the paper is given in Tab. I.

II. System Model and Preliminaries

In this section, we first present the proposed network setup that considers both uniform SBS deployment (see Fig. 1a)) and Stienen's cell based SBS deployment (see Fig. 1b)). Then mathematical preliminaries, which will be used for the evaluation of coverage performance in Sec. III, are introduced.

A. Network Layout

This paper considers a two-tier HetNet comprising of MBSs, SBSs, MBS-AUs, and SBS-AUs deployed according to the following two models. As per the uniform SBS deployment model (see Fig. 1a)), MBS-AUs, SBS-AUs, MBSs, and SBSs are distributed through PPPs $\phi_{\nu,\mathrm{M}}$, $\phi_{\nu,\mathrm{S}}$, ϕ_{M}, and ϕ_{S} (represented by pentagrams, asterisks, dots, and triangles), respectively. Conversely, in Stienen's cell based SBS deployment model (see Fig. 1b)), MBS-AUs, SBS-AUs, and MBSs are distributed via PPPs $\phi_{\nu,\mathrm{M}}$, $\phi_{\nu,\mathrm{S}}$, and ϕ_{M} (represented by pentagrams, asterisks, and dots), respectively, whereas SBSs are distributed via PHP $\vec{\phi}_{\mathrm{S}}$ (represented by triangles). The proposed setup considers dense urban scenarios [28], [29]. In our envisaged network layout, there is significant co-channel interference (to be derived in (6)) among the BSs when they use the same frequency band, and vice versa [5], [8], [19].

Consider a reference user[2] and assume that it is located at the origin of the coordinates of the network layout. The probability density function (PDF) that the RU is located

[2]The Slivnyak theorem states that an RU at the origin retains and simplifies the statistical properties of a PPP [11].

at distance r_{M} away from its serving MBS is given by $f_{r_{\mathrm{M}}}(r_{\mathrm{M}}) = 2\pi\lambda_{\mathrm{M}} r_{\mathrm{M}} \exp\left(-\pi\lambda_{\mathrm{M}} r_{\mathrm{M}}^2\right)$, where $r_{\mathrm{M}} > 0$ [30]. The effect of noise is ignored due to interference dominance. The Stienen's cell radius around MBS is denoted by $R_\circ$ and is equal to half of the distance between two closest MBSs, as shown in Fig. 1b). Furthermore, let d_1 and d_2 denote the coverage limits of MBS center-region, A^c_{M}, and MBS outer-region, A^o_{M}, respectively, in the uniform SBS deployment scenario. The distance between the closest MBSs is denoted by $R_\circ \Delta^{-1}$, where $\Delta = 1/2$ is a constant and its value is chosen based on Stienen's cell definition (see Subsec. II-B).
The PDF of $R_\circ$ can be written as

$$f_{R_\circ}(R_\circ) = 2\pi\lambda_{\mathrm{M}} R_\circ \Delta^{-2} \exp\left(-\pi\lambda_{\mathrm{M}} \left(R_\circ/\Delta\right)^2\right). \quad (1)$$

Lemma 1. *In a two-tier HetNet with Stienen's cell based SBS deployment, the SBS density can be expressed as $p\lambda_S$ [18], where*

$$p = \left(1 + \Delta^2\right)^{-1}. \quad (2)$$

Definition 1. *(Poisson hole process) Let ϕ_1 and ϕ_2 be two PPPs with intensities λ_1 and λ_2, respectively. Further, let*

$$\Xi \triangleq \bigcup \{x \in \phi_1 : b(x, r)\} \quad (3)$$

be the union of all disks of radius r centered at a point of ϕ_1. The PHP is defined as

$$\phi \triangleq \phi_2 \backslash \Xi. \quad (4)$$

In the PHP, each point in ϕ_1 carves out a hole of radius r from ϕ_2 [11].

B. Overview of Stienen's Model

Stienen's model can be constructed using Poisson-Voronoi tessellation (e.g., see Fig. 1) [31]. Assuming the closest BS association principle, the union of all MBS coverage areas forms a Voronoi tessellation [18], [32]. From Fig. 1b), we can observe that each Voronoi cell confines the MBS coverage area [25], [33]. The Stienen's cell around MBS is smaller than its coverage area [19]. This implies that each Voronoi cell is made up of Stienen's cell and its complementary area [25], [31], [33], [34]. This Voronoi cell division allows us to deploy BSs in these two areas with different densities [21], [32]. As MBSs have variable coverage areas, the exclusion disc via Stienen's model naturally captures the impact of the cell size [18]. Furthermore, Stienen's model also intrinsically captures the irregularity in distances to different cell edges [19].

C. Stienen's Cell based SBS Deployment

In this work, we use Stienen's cell based SBS deployment, where SBSs are employed outside the circular disk of radius $R_\circ$ around MBS using PHP, as indicated in Fig. 1b) [25], [33]. The region inside the circular disk is termed as cell interior region, A^c_z, while the region outside the Stienen's disk is denoted as cell edge region, A^o_z, of the zBS $\forall z \in$ (M,S). According to Stienen's model, $R_\circ$ around MBS is assumed to be random. The performance of the RU is analyzed in both inside and outside the disk around MBS. Moreover, in Fig. 1b),

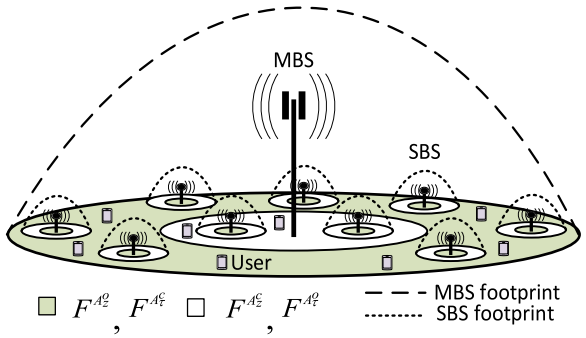

Fig. 2: A uniform SBS deployment model with SFR employment. According to SFR, the white and green colors distinguish the frequency band used in that region. In this figure, z and τ denote zBS and τBS, respectively, s.t., $\tau \in$ (M, S) and $z \in$ (M, S), $\forall\ \tau \neq z$ simultaneously. This principal of SFR also applies to Stienen's cell based SBS deployment model of Fig. 1b).

TABLE II: Frequency distribution using SFR

BS type	Edge region	Interior region
zBS	$F^{A^o_z}$	$F^{A^c_z}$
τBS	$F^{A^o_\tau}$	$F^{A^c_\tau}$

D is the distance between the closest interfering MBS and the RU, and $r_{\mathrm{M}} = \phi R_\circ$ represents the distance between the MBS and the RU. Furthermore, in conjunction with the proposed setup, we use SFR to further reduce interference and improve network performance.

D. Soft Frequency Reuse

Traditional cellular networks follow frequency division duplex to mitigate MBS-I [11]. In HetNets, higher throughput is achieved by aggressive[3] frequency reuse. However, this leads to severe MBS-I. Hence, a proactive interference mitigation and efficient resource allocation scheme is required to abate such interference. Herein, we introduce SFR to mitigate MBS-I in HetNets. According to SFR, the frequencies allocated to an MBS in A^c_{M} and A^o_{M} are used alternatively by SBSs in A^o_{S} and A^c_{S}, respectively. For example, the bandwidth F of 10 MHz is divided into two sub-bands with identical bandwidth, i.e., $F^{A^c_z}$ and $F^{A^o_\tau}$ [14], s.t., $\left(F^{A^c_z} = F^{A^o_\tau} = 5\text{ MHz}\right)$ and $\left(F^{A^c_z} \bigcap F^{A^o_\tau} = \phi\right)$ [in terms of band similarity] (see Fig. 2 and Tab. II). The SFR sub-bands are used in alternate regions by zBS and τBS, s.t., complete frequency band $F = F^{A^c_\tau} \bigcup F^{A^o_z}$ [24]. In this paper, SFR could apply to both uniform SBS deployment model (see Fig. 1a)) and the Stienen's cell based SBS deployment model (see Fig. 1b)).

III. Analysis of Coverage Probability

In this section, we derive coverage probability expressions for the following four network scenarios: (i) uniform SBS deployment with and without SFR (see Subsec. III-A and III-B), and (ii) Stienen's cell based SBS deployment model with and without SFR (see Subsec. III-C and III-D). Moreover,

[3]The term 'aggressive' implies the frequency reuse factor of 1.

the performance of the RU is investigated in both (i) inside Stienen's cell and (ii) outside Stienen's cell, as shown in Fig. 1b).

A. Coverage Probability for Uniform SBS Deployment with SFR

In the uniform SBS deployment scenario, we distribute SBSs according to a ϕ_s in an MBS coverage area together with SFR to reduce interference, as shown in Fig. 1a). The coverage probability expression, $P^{cov*}_{A^c_z,\zeta}(\beta_z)$, for the uniform SBS deployment with SFR where the RU is located in A^c_z can be obtain as

$$P^{cov*}_{A^c_z,\zeta}(\beta_z) = P\left(\text{SIR}^{D_L}_z > \beta_z\right). \tag{5}$$

Here, β_z is the SIR threshold while $\text{SIR}^{D_L}_z$ represents the D_L received SIR from zBS. $\text{SIR}^{D_L}_z$ can be expressed as

$$\text{SIR}^{D_L}_z = \frac{P^{D_L}_z |h_z| {r_z}^{-\alpha}}{I^{D_L}_{\phi_z,A^c_z} + I^{U_L}_{\phi_{\nu,z},A^c_z} + I^{D_L}_{\phi_\tau,A^o_\tau} + I^{U_L}_{\phi_{\nu,\tau},A^o_\tau}}, \tag{6}$$

where $P^{D_L}_z$ is the downlink transmit power by zBS and α is the path loss exponent. Due to SFR employment, the received D_L interference is the sum of (i) D_L interference from z-tier, $I^{D_L}_{\phi_z,A^c_z}$, (ii) D_L interference from τ-tier, $I^{D_L}_{\phi_\tau,A^o_\tau}$, (iii) uplink ($U_L$) interference from zBS-AUs, $I^{U_L}_{\phi_{\nu,z},A^c_z}$, and (iv) U_L interference from τBS-AUs, $I^{U_L}_{\phi_{\nu,\tau},A^o_\tau}$, respectively. Moreover, $z \in \{\text{M}, \text{S}\}$ and r_z represents the distance between the serving zBS and the RU.

$$\text{SIR}^{D_L}_z = \frac{P^{D_L}_z |h_z| {r_z}^{-\alpha}}{\sum\limits_{j\in\phi_z} P^{D_L}_j |h_j| r_j^{-\alpha} + \sum\limits_{j\in\phi_{\nu,z}} P^{U_L}_j |h_j| r_j^{-\alpha} + \sum\limits_{k\in\phi_\tau} P^{D_L}_k |h_k| r_k^{-\alpha} + \sum\limits_{k\in\phi_{\nu,\tau}} P^{U_L}_k |h_k| r_k^{-\alpha}}. \tag{7}$$

By substituting (6) into (5), we obtain $P^{cov*}_{A^c_z,\zeta}(\beta_z)$ as

$$\begin{aligned}
P^{cov*}_{A^c_z,\zeta}(\beta_z) &\overset{(1)}{=} P\left(\frac{P^{D_L}_z |h_z| {r_z}^{-\alpha}}{I^{D_L}_{\phi_z,A^c_z} + I^{U_L}_{\phi_{\nu,z},A^c_z} + I^{D_L}_{\phi_\tau,A^o_\tau} + I^{U_L}_{\phi_{\nu,\tau},A^o_\tau}} > \beta_z\right) \\
&\overset{(2)}{=} \text{E}_{r_z, I^{D_L}_{\phi_z,A^c_z}, I^{U_L}_{\phi_{\nu,\tau},A^o_\tau}} \\
&\times \left[\exp\left(-\frac{r^\alpha_z \beta_z}{P^{D_L}_z}\left(I^{D_L}_{\phi_z,A^c_z} + I^{U_L}_{\phi_{\nu,z},A^c_z} + I^{D_L}_{\phi_\tau,A^o_\tau} + I^{U_L}_{\phi_{\nu,\tau},A^o_\tau}\right)\right)\right] \\
&\overset{(3)}{=} \text{E}_{r_z, I^{D_L}_{\phi_z,A^c_z}, I^{U_L}_{\phi_{\nu,\tau},A^o_\tau}} \\
&\times \left[\exp\left(-s\left(I^{D_L}_{\phi_z,A^c_z} + I^{U_L}_{\phi_{\nu,z},A^c_z} + I^{D_L}_{\phi_\tau,A^o_\tau} + I^{U_L}_{\phi_{\nu,\tau},A^o_\tau}\right)\right)\right]\Big|_{s=\frac{r^\alpha_z\beta_z}{P^{D_L}_z}} \\
&\overset{(4)}{=} \text{E}_{r_z}\left[\text{E}_{I^{D_L}_{\phi_z,A^c_z}} \exp\left(-s\left(I^{D_L}_{\phi_z,A^c_z}\right)\right) \times \text{E}_{I^{U_L}_{\phi_{\nu,z},A^c_z}} \exp\left(-s\left(I^{U_L}_{\phi_{\nu,z},A^c_z}\right)\right)\right. \\
&\left. \times\, \text{E}_{I^{D_L}_{\phi_z,A^o_\tau}} \exp\left(-s\left(I^{D_L}_{\phi_z,A^o_\tau}\right)\right) \times \text{E}_{I^{U_L}_{\phi_{\nu,\tau},A^o_\tau}} \exp\left(-s\left(I^{U_L}_{\phi_{\nu,\tau},A^o_\tau}\right)\right)\right] \\
&\overset{(5)}{=} \text{E}_{r_z}\left[\mathcal{L}_{I^{D_L}_{\phi_z,A^c_z}}(s) \times \mathcal{L}_{I^{U_L}_{\phi_{\nu,z},A^c_z}}(s) \times \mathcal{L}_{I^{D_L}_{\phi_\tau,A^o_\tau}}(s) \times \mathcal{L}_{I^{U_L}_{\phi_{\nu,\tau},A^o_\tau}}(s)\right].
\end{aligned} \tag{8}$$

Here, Step (1) follows up the coverage probability definition [5]. Step (2) follows up Step (1) (the proof of Step (2) is given in Appendix A). In Step (2), the expression, $\text{E}_{r_z, I^{D_L}_{\phi_z,A^c_z}, I^{U_L}_{\phi_v,\tau,A^o_\tau}}$, indicates the expectation with respect to five different random variables which are (i) the distance between the RU and its associated BS, r_z, (ii) the total D_L interference from other BSs in A^c_z, $I^{D_L}_{\phi_z,A^c_z}$, (iii) the total U_L interference received from other users in A^c_z, $I^{U_L}_{\phi_{\nu,z},A^c_z}$, (iv) the total D_L interference from other BSs in A^o_τ, $I^{D_L}_{\phi_\tau,A^o_\tau}$, and (v) the total U_L interference received from other users in A^o_τ, $I^{U_L}_{\phi_v,\tau,A^o_\tau}$. Similarly, we reach Step (3) by substituting $r^\alpha_z\beta_z/P^{D_L}_z$ with s. Moreover, Step (4) is derived based on Step (3) by using the exponential property of transforming sums into products, i.e., $\exp(a+b) = \exp(a)\times\exp(b)$. Lastly, Step (5) is achieved from Step (4) by following Laplace transform (LT) definition [4]. Here, it is worth mentioning that we transform Step (3) into Step (4) considering the fact that Step (4) can be easily converted to Step (5) by a similar procedure as presented on pages 14-16 of [11].

1) Coverage probability of uniform SBS deployment with SFR for MBS-AU in A^c_M: The coverage probability of uniform SBS deployment for MBS-AU in A^c_M with SFR employment, $P^{cov*}_{A^c_\text{M}}(\beta_\text{M})$, is given as

$$P^{cov*}_{A^c_\text{M}}(\beta_\text{M}) = \text{E}_{r_\text{M}}\left[\mathcal{L}_{I^{D_L}_{\phi_\text{M},A^c_\text{M}}}(s) \times \mathcal{L}_{I^{U_L}_{\phi_{\nu,\text{M}},A^c_\text{M}}}(s) \times \mathcal{L}_{I^{D_L}_{\phi_\text{S},A^o_\text{S}}}(s) \times \mathcal{L}_{I^{U_L}_{\phi_{\nu,\text{S}},A^o_\text{S}}}(s)\right]. \tag{9}$$

The LT of the interference from MBS-tier in D_L is obtained as

$$\begin{aligned}
\mathcal{L}_{I^{D_L}_{\phi_\text{M},A^c_\text{M}}}(s) &\overset{(a)}{=} \text{E}_{I^{D_L}_{\phi_\text{M},A^c_\text{M}}}\left[\exp\left(-I^{D_L}_{\phi_\text{M},A^c_\text{M}} s\right)\right]|_{s=r^\alpha_\text{M}\beta_\text{M}} \\
&\overset{(b)}{=} \text{E}_{I^{D_L}_{\phi_\text{M},A^c_\text{M}},|h_j|}\left[\exp\left(-s\sum_{j\in\phi_\text{M}} |h_j| r_j^{-\alpha}\right)\right] \\
&\overset{(c)}{=} \text{E}_{I^{D_L}_{\phi_\text{M},A^c_\text{M}},|h_j|}\left[\prod_{j\in\phi_\text{M}} \exp\left(-|h_j|\beta_\text{M} r^\alpha_\text{M} r_j^{-\alpha}\right)\right] \\
&\overset{(d)}{=} \text{E}_{I^{D_L}_{\phi_\text{M},A^c_\text{M}}}\left[\prod_{j\in\phi_\text{M}} \text{E}_{|h_j|}\exp\left(-|h_j|\beta_\text{M} r^\alpha_\text{M} r_j^{-\alpha}\right)\right] \\
&\overset{(e)}{=} \text{E}_{I^{D_L}_{\phi_\text{M},A^c_\text{M}}}\left[\prod_{j\in\phi_\text{M}} \frac{1}{1+\beta_\text{M}\left(\frac{r_j}{r_\text{M}}\right)^{-\alpha}}\right] \\
&\overset{(f)}{=} \exp\left(-2\pi\lambda_\text{M}\int_{y'}^{d1} \frac{r_j dr_j}{1+\left(r_j r_\text{M}^{-1}\beta_\text{M}^{-1/\alpha}\right)^\alpha}\right) \\
&\overset{(g)}{=} \exp\left(-\pi\lambda_\text{M}\beta_\text{M}^{2/\alpha} r^2_\text{M}\int_{\left(\frac{y'}{\beta_\text{M}^{1/\alpha} r_\text{M}}\right)^2}^{\left(\frac{d_1}{\beta_\text{M}^{1/\alpha} r_\text{M}}\right)^2} \frac{du}{1+(u)^{\alpha/2}}\right)
\end{aligned}$$

$$P^{cov*}_{A^c_{\rm M},\zeta}(\beta_{\rm M}) = \frac{2\pi\lambda_{\rm M}}{1-\exp\left(-\lambda_{\rm M}\pi d_1^2\right)} \int_0^{d_1} \exp\left(\frac{\lambda_{\rm M} Q}{d_1^{(\alpha-2)}} \mathcal{J}\left(\alpha, -\beta_{\rm M}\left(\frac{r_{\rm M}}{d_1}\right)^{\alpha}\right) - \frac{\lambda_{\rm M} Q}{y'^{(\alpha-2)}} \mathcal{J}\left(\alpha, -\beta_{\rm M}\left(\frac{r_{\rm M}}{y'}\right)^{\alpha}\right) + \frac{\lambda_{\nu,{\rm M}} Q\eta_1}{d_1^{(\alpha-2)}} \mathcal{J}\left(\alpha, -\beta_{\rm M}\eta_1 \left(\frac{r_{\rm M}}{d_1}\right)^{\alpha}\right) - \frac{\lambda_{\nu,{\rm M}} Q\eta_1}{y'^{(\alpha-2)}} \mathcal{J}\left(\alpha, -\beta_{\rm M}\eta_1 \left(\frac{r_{\rm M}}{y'}\right)^{\alpha}\right) - \frac{\lambda_{\rm S} Q\eta_2}{d_1^{(\alpha-2)}} \mathcal{J}\left(\alpha, -\beta_{\rm M}\eta_2 \left(\frac{r_{\rm M}}{d_1}\right)^{\alpha}\right) - \frac{\lambda_{\nu,{\rm S}} Q\eta_3}{d_1^{(\alpha-2)}} \mathcal{J}\left(\alpha, -\beta_{\rm M}\eta_3 \left(\frac{r_{\rm M}}{d_1}\right)^{\alpha}\right) - \lambda_{\rm M}\pi r_{\rm M}^2 \right) r_{\rm M} dr_{\rm M}. \tag{12}$$

$$P^{cov*}_{A^o_{\rm M},\zeta}(\beta_{\rm M}) = \frac{2\pi\lambda_{\rm M}}{\exp\left(-\lambda_{\rm M}\pi d_1^2\right)} \int_{d_1}^{\infty} \exp\left(-\frac{\lambda_{\rm M} Q}{d_1^{(\alpha-2)}} \mathcal{J}\left(\alpha, -\beta_{\rm M}\left(\frac{r_{\rm M}}{d_1}\right)^{\alpha}\right) - \frac{\lambda_{\nu,{\rm M}} Q\eta_1}{d_1^{(\alpha-2)}} \mathcal{J}\left(\alpha, -\beta_{\rm M}\eta_1 \left(\frac{r_{\rm M}}{d_1}\right)^{\alpha}\right) - \frac{\lambda_{\rm S} Q\eta_2}{d_1^{(\alpha-2)}} \mathcal{J}\left(\alpha, -\beta_{\rm M}\eta_2 \left(\frac{r_{\rm M}}{d_1}\right)^{\alpha}\right) - \frac{\lambda_{\nu,{\rm S}} Q\eta_3}{d_1^{(\alpha-2)}} \mathcal{J}\left(\alpha, -\beta_{\rm M}\eta_3 \left(\frac{r_{\rm M}}{d_1}\right)^{\alpha}\right) - \lambda_{\rm M}\pi r_{\rm M}^2 \right) r_{\rm M} dr_{\rm M}. \tag{13}$$

$$\overset{(h)}{=} \exp\Bigg(\lambda_{\rm M} Q d_1^{(2-\alpha)} {}_2F_1\left(1, 1-\frac{2}{\alpha}, 2-\frac{2}{\alpha}, -\beta_{\rm M}\left(\frac{r_{\rm M}}{d_1}\right)^{\alpha}\right) - \lambda_{\rm M} Q y'^{(2-\alpha)} {}_2F_1\left(1, 1-\frac{2}{\alpha}, 2-\frac{2}{\alpha}, -\beta_{\rm M}\left(\frac{r_{\rm M}}{y'}\right)^{\alpha}\right)\Bigg). \tag{10}$$

In (10), Step (a) is achieved from the definition of LT [4]. Step (b) follows up Step (a) by replacing $I^{U_L}_{\phi_{\rm M},A^c_{\rm M}} = \sum_{l\in\phi_{\rm M}} P^{U_L}_{t,l}|h_l|r_l^{-\alpha}$ into Step (a). Step (c) is achieved by replacing the value of s with $r_{\rm M}^{\alpha}\beta_{\rm M}$ into Step (b). Step (e) follows up Step (d) by evaluating LT in terms of h_j. Step (f) is obtained based on the probability generating functional (PGFL) definition of PPP [11]. Moreover, Step (g) is achieved by replacing u with $\left(r_j/\beta_{\rm M}^{1/\alpha} r_{\rm M}\right)^2$ into Step (f). Lastly, we reach Step (h) through the Gauss-hypergeometric approximation of Step (g) where ${}_2F_1(\cdot)$ denotes the Gauss-hypergeometric function [5]. In Step (h), $Q = \frac{\pi\beta_{\rm M} r_{\rm M}^{\alpha}}{\alpha/2-1}$.

Similarly, the LT of the interference from MBS-AUs in U_L, $\mathcal{L}_{I^{U_L}_{\phi_{\nu,{\rm M}},A^c_{\rm M}}}(s)$, is obtain as

$$\mathcal{L}_{I^{U_L}_{\phi_{\nu,{\rm M}},A^c_{\rm M}}}(s) = \exp\Bigg(\lambda_{\nu,{\rm M}} Q\eta_1 d_1^{(2-\alpha)} {}_2F_1\left(1, 1-\frac{2}{\alpha}, 2-\frac{2}{\alpha}, -\beta_{\rm M}\left(\frac{r_{\rm M}}{d_1}\right)^{\alpha}\right) - \lambda_{\nu,{\rm M}} Q\eta_1 y'^{(2-\alpha)} {}_2F_1\left(1, 1-\frac{2}{\alpha}, 2-\frac{2}{\alpha}, -\beta_{\rm M}\left(\frac{r_{\rm M}}{y'}\right)^{\alpha}\right)\Bigg). \tag{11}$$

Here, $\eta_1 = P^{U_L}_{\nu,{\rm M}}/P^{D_L}_{\rm M}$, where $P^{U_L}_{\nu,{\rm M}}$ is the transmit power of MBS-AUs in U_L and $P^{D_L}_{\rm M}$ is transmit power of MBS in D_L.

The LT of the interference from SBS-tier in D_L, $\mathcal{L}_{I^{D_L}_{\phi_{\rm S},A^o_{\rm S}}}(s)$, is obtain as

$$\mathcal{L}_{I^{D_L}_{\phi_{\rm S},A^o_{\rm S}}}(s) = {\rm E}_{I^{D_L}_{\phi_{\rm S},A^o_{\rm S}}}\left[\exp\left(-I^{D_L}_{\phi_{\rm S},A^o_{\rm S}} s\right)\right]\Big|_{s=\frac{r_z^{\alpha}\beta_{\rm M}}{P^{D_L}_{\rm M}}}$$

$$= {\rm E}_{I^{D_L}_{\phi_{\rm S},A^o_{\rm S}},|h_k|}\left[\exp\left(-s\sum_{k\in\phi_\tau} P_s^{D_L}|h_k|r_k^{-\alpha}\right)\right]$$

$$= {\rm E}_{I^{D_L}_{\phi_{\rm S},A^o_{\rm S}},|h_k|}\left[\prod_{k\in\phi_\tau}\exp\left(-|h_k|\beta_{\rm M}\eta_2 r_{\rm M}^{\alpha} r_k^{-\alpha}\right)\right]$$

$$= {\rm E}_{I^{D_L}_{\phi_{\rm S},A^o_{\rm S}}}\left[\prod_{k\in\phi_\tau}{\rm E}_{|h_k|}\exp\left(-|h_k|\beta_{\rm M}\eta_2 r_{\rm M}^{\alpha} r_k^{-\alpha}\right)\right]$$

$$= {\rm E}_{I^{D_L}_{\phi_{\rm S},A^o_{\rm S}}}\left[\prod_{k\in\phi_\tau}\frac{1}{1+\beta_{\rm M}\eta_2\left(\frac{r_k}{r_{\rm M}}\right)^{-\alpha}}\right]$$

$$= \exp\left(-2\pi\lambda_{\rm S}\int_{d1}^{\infty}\frac{r_k dr_k}{1+\left(\frac{r_k}{\left(\eta_2\beta_{\rm M}\right)^{1/\alpha} r_{\rm M}}\right)^{\alpha}}\right)$$

$$= \exp\left(-\pi\lambda_{\rm S}\eta_2^{2/\alpha}\beta_{\rm M}^{2/\alpha} r_{\rm M}^2\int_{\left(\frac{d1}{\left(\eta_2\beta_{\rm M}\right)^{1/\alpha} r_{\rm M}}\right)^2}^{\infty}\frac{du}{1+(u)^{\alpha/2}}\right)$$

$$= \exp\Bigg(-\lambda_{\rm S} Q\eta_2 d_1^{(2-\alpha)} \times {}_2F_1\left(1, 1-2/\alpha, 2-2/\alpha, -\beta_{\rm M}\eta_2\left(\frac{r_{\rm M}}{d_1}\right)^{\alpha}\right)\Bigg). \tag{14}$$

Here, $\eta_2 = P^{D_L}_{\rm S}/P^{D_L}_{\rm M}$, where $P^{D_L}_{\rm S}$ is the transmit power of SBSs in D_L.

Similarly, the LT of the interference from SBS-AUs in U_L, $\mathcal{L}_{I^{U_L}_{\phi_{\nu,{\rm S}},A^o_{\rm S}}}(s)$, can be obtained as

$$\mathcal{L}_{I^{U_L}_{\phi_{\nu,{\rm S}},A^o_{\rm S}}}(s) = \exp\Bigg(-\lambda_{\nu,{\rm S}} Q\eta_3 d_1^{(2-\alpha)} \times {}_2F_1\left(1, 1-2/\alpha, 2-2/\alpha, -\beta_{\rm M}\eta_3\left(\frac{r_{\rm M}}{d_1}\right)^{\alpha}\right)\Bigg). \tag{15}$$

Here, $\eta_3 = P^{U_L}_{u,{\rm S}}/P^{D_L}_{\rm M}$, where $P^{U_L}_{u,{\rm S}}$ is the transmit power of SBS-AUs in U_L.

$RU_{A^c_{\rm M}}$ and $RU_{A^o_{\rm M}}$ associating with MBS located at distance $r_{\rm M}$ have PDFs given, respectively, as [35]

$$f_{r_{\rm M}|RU_{A^c_{\rm M}}}(r_{\rm M}) = \frac{2\pi\lambda_{\rm M} r_{\rm M}\exp\left(-\lambda_{\rm M}\pi r_{\rm M}^2\right)}{1-\exp\left(-\lambda_{\rm M}\pi d_1^2\right)}, \tag{16}$$

and

$$f_{r_{\rm M}|RU_{A^o_{\rm M}}}(r_{\rm M}) = \frac{2\pi\lambda_{\rm M} r_{\rm M}\exp\left(-\lambda_{\rm M}\pi r_{\rm M}^2\right)}{\exp\left(-\lambda_{\rm M}\pi d_1^2\right)}. \tag{17}$$

$$P^{cov}_{A^c_{\mathrm{M}},\zeta}(\beta_{\mathrm{M}}) = \frac{2\pi\lambda_{\mathrm{M}}}{1-\exp\left(-\lambda_{\mathrm{M}}\pi d_1^2\right)} \int_0^{d_1} \exp\left(2\times\left(\frac{\lambda_{\mathrm{M}}\pi\beta_{\mathrm{M}} d_1^{(2-\alpha)} r_{\mathrm{M}}^{\alpha}}{\alpha/2-1}\mathcal{J}\left(\alpha,-\beta_{\mathrm{M}}\left(\frac{r_{\mathrm{M}}}{d_1}\right)^{\alpha}\right) - \frac{\lambda_{\mathrm{M}}\pi\beta_{\mathrm{M}} y'^{(2-\alpha)} r_{\mathrm{M}}^{\alpha}}{\alpha/2-1}\right.\right.$$
$$\mathcal{J}\left(\alpha,-\beta_{\mathrm{M}}\left(\frac{r_{\mathrm{M}}}{y'}\right)^{\alpha}\right) + \frac{\lambda_{\nu,\mathrm{M}}\pi\beta_{\mathrm{M}}\eta_1 d_1^{(2-\alpha)} r_{\mathrm{M}}^{\alpha}}{\alpha/2-1}\mathcal{J}\left(\alpha,-\beta_{\mathrm{M}}\eta_1\left(\frac{r_{\mathrm{M}}}{d_1}\right)^{\alpha}\right) - \frac{\lambda_{\nu,\mathrm{M}}\pi\beta_{\mathrm{M}}\eta_1 y'^{(2-\alpha)} r_{\mathrm{M}}^{\alpha}}{\alpha/2-1}\mathcal{J}\left(\alpha,-\beta_{\mathrm{M}}\eta_1\left(\frac{r_{\mathrm{M}}}{y'}\right)^{\alpha}\right)$$
$$\left.\left. - \frac{\lambda_{\mathrm{S}}\pi\eta_2\beta_{\mathrm{M}} d_1^{(2-\alpha)} r_{\mathrm{M}}^{\alpha}}{\alpha/2-1}\mathcal{J}\left(\alpha,-\beta_{\mathrm{M}}\eta_2\left(\frac{r_{\mathrm{M}}}{d_1}\right)^{\alpha}\right) - \frac{\lambda_{\nu,\mathrm{S}}\pi\eta_3\beta_{\mathrm{M}} d_1^{(2-\alpha)} r_{\mathrm{M}}^{\alpha}}{\alpha/2-1}\mathcal{J}\left(\alpha,-\beta_{\mathrm{M}}\eta_3\left(\frac{r_{\mathrm{M}}}{d_1}\right)^{\alpha}\right) - \lambda_{\mathrm{M}}\pi r_{\mathrm{M}}^2\right)\right) r_{\mathrm{M}} dr_{\mathrm{M}}. \quad (19)$$

$$P^{cov}_{A^o_{\mathrm{M}},\zeta}(\beta_{\mathrm{M}}) = \frac{2\pi\lambda_{\mathrm{M}}}{\exp\left(-\lambda_{\mathrm{M}}\pi d_1^2\right)} \int_{d_1}^{\infty} \exp\left(2\times\left(-\frac{\lambda_{\mathrm{M}}\pi\beta_{\mathrm{M}} d_1^{(2-\alpha)} r_{\mathrm{M}}^{\alpha}}{\alpha/2-1}\mathcal{J}\left(\alpha,-\beta_{\mathrm{M}}\left(\frac{r_{\mathrm{M}}}{d_1}\right)^{\alpha}\right) - \frac{\lambda_{\mathrm{M}}\pi\beta_{\mathrm{M}}\eta_1 d_1^{(2-\alpha)} r_{\mathrm{M}}^{\alpha}}{\alpha/2-1}\mathcal{J}\left(\alpha,-\beta_{\mathrm{M}}\eta_1\left(\frac{r_{\mathrm{M}}}{d_1}\right)^{\alpha}\right)\right.\right.$$
$$\left.\left. - \frac{\lambda_{\mathrm{S}}\pi\eta_2\beta_{\mathrm{M}} d_1^{(2-\alpha)} r_{\mathrm{M}}^{\alpha}}{\alpha/2-1}\mathcal{J}\left(\alpha,-\beta_{\mathrm{M}}\eta_2\left(\frac{r_{\mathrm{M}}}{d_1}\right)^{\alpha}\right) - \frac{\lambda_{\nu,\mathrm{S}}\pi\eta_3\beta_{\mathrm{M}} d_1^{(2-\alpha)} r_{\mathrm{M}}^{\alpha}}{\alpha/2-1}\mathcal{J}\left(\alpha,-\beta_{\mathrm{M}}\eta_3\left(\frac{r_{\mathrm{M}}}{d_1}\right)^{\alpha}\right) - \lambda_{\mathrm{M}}\pi r_{\mathrm{M}}^2\right)\right) r_{\mathrm{M}} dr_{\mathrm{M}}. \quad (20)$$

The coverage probability expression of uniform SBS deployment with SFR for MBS associated RU in A^c_{M}, $P^{cov*}_{A^c_{\mathrm{M}},\zeta}(\beta_{\mathrm{M}})$, can be written as [8], [35]

$$P^{cov*}_{A^c_{\mathrm{M}},\zeta}(\beta_{\mathrm{M}}) = \int_{y'}^{d_1} \mathcal{L}_{I^{D_L}_{\phi_{\mathrm{M}},A^c_{\mathrm{M}}}}(s)\,\mathcal{L}_{I^{U_L}_{\phi_{\nu,\mathrm{M}},A^c_{\mathrm{M}}}}(s)\,\mathcal{L}_{I^{D_L}_{\phi_{\tau},A^o_{\mathrm{S}}}}(s)\,\mathcal{L}_{I^{U_L}_{\phi_{\nu,\mathrm{S}},A^o_{\mathrm{S}}}}(s)\, f_{r_{\mathrm{M}}|U_{A^c_{\mathrm{M}}}}(r_{\mathrm{M}})\, dr_{\mathrm{M}}. \quad (18)$$

By substituting (10), (11), (14), (15) and (16) into (18), we obtain $P^{cov*}_{A^c_{\mathrm{M}},\zeta}(\beta_{\mathrm{M}})$ as (12). In (12), $\mathcal{J}(\cdot)$ is the Gauss-hypergeometric function. The same applies to all $\mathcal{J}(\cdot)$ in the rest of the paper.

2) Coverage probability of uniform SBS deployment with SFR for MBS-AU in A^o_M: The coverage probability expression of uniform SBS deployment with SFR for MBS associated RU in A^o_{M}, $P^{cov*}_{A^o_{\mathrm{M}},\zeta}(\beta_{\mathrm{M}})$, can be written as [8]

$$P^{cov*}_{A^o_{\mathrm{M}},\zeta}(\beta_{\mathrm{M}}) = \int_{d_1}^{\infty} \mathcal{L}_{I^{D_L}_{\phi_{\mathrm{M}},A^o_{\mathrm{M}}}}(s)\,\mathcal{L}_{I^{U_L}_{\phi_{\nu,\mathrm{M}},A^o_{\mathrm{M}}}}(s)\,\mathcal{L}_{I^{D_L}_{\phi_{\tau},A^c_{\mathrm{S}}}}(s)\,\mathcal{L}_{I^{U_L}_{\phi_{\nu,\mathrm{S}},A^c_{\mathrm{S}}}}(s)\, f_{r_{\mathrm{M}}|RU_{A^o_{\mathrm{M}}}}(r_{\mathrm{M}})\, dr_{\mathrm{M}}. \quad (21)$$

Using the approach similar to (12), the coverage probability expression of uniform SBS deployment for MBS associated RU in A^o_{S} with SFR employment, $P^{cov*}_{A^o_{\mathrm{S}},\zeta}(\beta_{\mathrm{MM}})$, can be given as (13).

B. Coverage Probability for Uniform SBS Deployment without SFR

In this subsection, *without SFR* implies that the entire MBS coverage area adopts the same frequency band and, thus, it leads to higher interference. By using the approach similar to (12) and (13), the coverage probability expressions of uniform SBS deployment without SFR for MBS associated RU in both A^c_{M} and A^o_{M}, i.e., $P^{cov}_{A^c_{\mathrm{M}},\zeta}(\beta_{\mathrm{M}})$, and $P^{cov}_{A^o_{\mathrm{M}},\zeta}(\beta_{\mathrm{M}})$, are given as (19) and (20), respectively.

C. Coverage Probability for SFR-enabled Stienen's Cell based SBS Deployment

Let us now consider SFR-enabled Stienen's cell based SBS deployment model with SFR. The expression for coverage probability, $P^{cov}_{A^c_z,\varrho}(\beta_z)$, can be written as

$$P^{cov}_{A^c_z,\varrho}(\beta_z) = P\left(\mathrm{SIR}^{D_L}_z > \beta_z\right), \quad (22)$$

where

$$\mathrm{SIR}^{D_L}_z = \frac{P^{D_L}_z |h_z| r_z^{-\alpha}}{I^{D_L}_{\phi_z,A^c_z} + I^{U_L}_{\phi_{\nu,z},A^c_z} + I^{D_L}_{\vec{\phi}_{\tau},A^o_{\tau}} + I^{U_L}_{\vec{\phi}_{\nu,\tau},A^o_{\tau}}}. \quad (23)$$

Here, $I^{D_L}_{\vec{\phi}_{\tau},A^o_{\tau}}$ and $I^{U_L}_{\vec{\phi}_{\nu,\tau},A^o_{\tau}}$ are the D_L and U_L interference received from τBS and τBS-AUs, respectively. Moreover, $\vec{\phi}_{\tau}$ and $\vec{\phi}_{\nu,\tau}$ are the PHP of τBS and τBS-AUs, respectively. Following the same procedure as we used for deriving (8), we obtain (24) from (22) as

$$P^{cov}_{A^c_z,\varrho}(\beta_z) = \mathrm{E}_{r_z,R_{\circ}}\left[\mathcal{L}_{I^{D_L}_{\phi_z,A^c_z}}(s)\times\mathcal{L}_{I^{U_L}_{\phi_{\nu,z},A^c_z}}(s)\times\mathcal{L}_{I^{D_L}_{\vec{\phi}_{\tau},A^o_{\tau}}}(s)\times\mathcal{L}_{I^{U_L}_{\vec{\phi}_{\nu,\tau},A^o_{\tau}}}(s)\right]. \quad (24)$$

1) Coverage probability of SFR-enabled Stienen's cell based SBS deployment for MBS-AU in A^c_M: The coverage probability of SFR-enabled Stienen's cell based SBS deployment for MBS-AU in A^c_{M}, $P^{cov}_{A^c_{\mathrm{M}},\varrho}(\beta_{\mathrm{M}})$, can be calculated as (29).

The coverage probability expression for MBS can be expressed from (24) as

$$P^{cov}_{A^c_{\mathrm{M}},\varrho}(\beta_{\mathrm{M}}) = \mathrm{E}_{r_{\mathrm{M}},R_{\circ}}\left[\mathcal{L}_{I^{D_L}_{\phi_{\mathrm{M}},A^c_{\mathrm{M}}}}(s)\times\mathcal{L}_{I^{U_L}_{\phi_{\nu,\mathrm{M}},A^c_{\mathrm{M}}}}(s)\times\mathcal{L}_{I^{D_L}_{\vec{\phi}_{\mathrm{S}},A^o_{\mathrm{S}}}}(s)\times\mathcal{L}_{I^{U_L}_{\vec{\phi}_{\nu,\mathrm{S}},A^o_{\mathrm{S}}}}(s)\right]\Big|_{s=\frac{r_z^{\alpha}\beta_{\mathrm{M}}}{P^{D_L}_{\mathrm{M}}}}. \quad (25)$$

From Fig. 1b), it is clear that the nearest interferer is located at distance D away from the $RU_{A^c_{\mathrm{M}}}$ and at a distance $R_{\circ}\Delta^{-1}$ away from the serving MBS. By applying the law of cosines and with minor simplifications, we obtain D as

$$P^{cov*}_{A^c_{\mathrm{M}},\varrho}(\beta_{\mathrm{M}})=\int_0^1 \left(\frac{2\Delta^{-2}\psi\left(1+\Delta^{-2}\right)}{\left(\Delta^{-2}+\psi^2\right)^2}\right)\left(\left(1+\beta_{\mathrm{M}}\left(\frac{\psi}{\left(\Delta^{-2}+\psi^2\right)^{1/2}}\right)^{\alpha}\right)\left(1+\eta_1\beta_{\mathrm{M}}\left(\frac{\psi}{\left(\Delta^{-2}+\psi^2\right)^{1/2}}\right)^{\alpha}\right)\right)^{-1}$$
$$\left(\left[1+\frac{\beta_{\mathrm{M}}\Delta^2\psi^{\alpha}}{\alpha/2-1}\left(\left(\Delta^{-1}-\psi\right)^{2-\alpha}\left(\mathcal{J}\left(\alpha,-\beta_{\mathrm{M}}\left(\frac{\psi}{\left(\Delta^{-1}-\psi\right)}\right)^{\alpha}\right)+\frac{\eta_1\lambda_{\nu,\mathrm{M}}}{\lambda_{\mathrm{M}}}\mathcal{J}\left(\alpha,-\eta_1\beta_{\mathrm{M}}\left(\frac{\psi}{\left(\Delta^{-1}-\psi\right)}\right)^{\alpha}\right)\right)+\right.\right.$$
$$\left.\left.\frac{\left(1-\psi\right)^{2-\alpha}}{\lambda_{\mathrm{M}}}\left(\vec{\lambda}_{\mathrm{S}}\eta_2\mathcal{J}\left(\alpha,-\eta_2\beta_{\mathrm{M}}\left(\frac{\psi}{\left(1-\psi\right)}\right)^{\alpha}\right)+\vec{\lambda}_{\nu,\mathrm{S}}\eta_3\mathcal{J}\left(\alpha,-\eta_3\beta_{\mathrm{M}}\left(\frac{\psi}{\left(1-\psi\right)}\right)^{\alpha}\right)\right)\right)\right]^2\right)^{-1}d\psi. \quad (29)$$

$$P^{cov*}_{A^c_{\mathrm{M}},\varrho}(\beta_{\mathrm{M}})=\int_1^{\infty} \left(\frac{2\psi\left(1+\Delta^{-2}\right)}{\left(\Delta^{-2}+\psi^2\right)^2}\right)\left(\left(1+\beta_{\mathrm{M}}\left(\frac{\psi}{\left(\Delta^{-2}+\psi^2\right)^{1/2}}\right)^{\alpha}\right)\left(1+\eta_1\beta_{\mathrm{M}}\left(\frac{\psi}{\left(\Delta^{-2}+\psi^2\right)^{1/2}}\right)^{\alpha}\right)\right)^{-1}$$
$$\left(\left[1+\frac{\beta_{\mathrm{M}}\Delta^2\psi^{\alpha}}{\alpha/2-1}\left(\left(\Delta^{-1}-\psi\right)^{2-\alpha}\left(\mathcal{J}\left(\alpha,-\beta_{\mathrm{M}}\left(\frac{\psi}{\left(\Delta^{-1}-\psi\right)}\right)^{\alpha}\right)+\frac{\eta_1\lambda_{\nu,\mathrm{M}}}{\lambda_{\mathrm{M}}}\mathcal{J}\left(\alpha,-\eta_1\beta_{\mathrm{M}}\left(\frac{\psi}{\left(\Delta^{-1}-\psi\right)}\right)^{\alpha}\right)\right)+\right.\right.$$
$$\left.\left.\frac{\left(1-\psi\right)^{2-\alpha}}{\lambda_{\mathrm{M}}}\left(\vec{\lambda}_{\mathrm{S}}\eta_2\mathcal{J}\left(\alpha,-\eta_2\beta_{\mathrm{M}}\left(\frac{\psi}{\left(1-\psi\right)}\right)^{\alpha}\right)+\vec{\lambda}_{\nu,\mathrm{S}}\eta_3\mathcal{J}\left(\alpha,-\eta_3\beta_{\mathrm{M}}\left(\frac{\psi}{\left(1-\psi\right)}\right)^{\alpha}\right)\right)\right)\right]^2\right)^{-1}d\psi. \quad (30)$$

$$D^2=R_{\circ}^2\Delta^{-2}+\left(\psi R_{\circ}\right)^2-2\Delta^{-1}\psi R_{\circ}^2\cos\left(\theta\right)$$
$$D=R_{\circ}\sqrt{\Delta^{-2}+\psi^2-2\Delta^{-1}\psi\cos\left(\theta\right)}$$
$$D\approx R_{\circ}\sqrt{\Delta^{-2}+\psi^2}. \quad (26)$$

Here, θ is the angle between r_{M} and $R_{\circ}\Delta^{-1}$, as shown in Fig. 1b). Moreover, θ is also uniformly distributed as locations of $RU_{A^c_{\mathrm{M}}}$. The LT of the closest interfering MBS from $RU_{A^c_{\mathrm{M}}}$ can be evaluated as

$$\mathcal{L}^{D}_{I^{D_L}_{\phi_{\mathrm{M}},A^c_{\mathrm{M}}}}(s)=\mathrm{E}_{I^{D_L}_{\phi_{\mathrm{M}},A^c_{\mathrm{M}}}}\left[\exp\left(-I^{D_L}_{\phi_{\mathrm{M}},A^c_{\mathrm{M}}}s\right)\right]\Big|_{s=\frac{r_{\mathrm{M}}^{\alpha}\beta_{\mathrm{M}}}{P_{\mathrm{M}}^{D_L}}}$$
$$=\mathrm{E}_{I^{D_L}_{\phi_{\mathrm{M}},A^c_{\mathrm{M}}},|h|}\left[\exp\left(-sP_{\mathrm{M}}^{D_L}|h|D^{-\alpha}\right)\right]$$
$$=\mathrm{E}_{I^{D_L}_{\phi_{\mathrm{M}},A^c_{\mathrm{M}}},|h|}\left[\exp\left(-|h|\beta_{\mathrm{M}}\left(\frac{\psi}{\left(\Delta^{-2}+\psi^2\right)^{1/2}}\right)^{\alpha}\right)\right]$$
$$=\mathrm{E}_{I^{D_L}_{\phi_{\mathrm{M}},A^c_{\mathrm{M}}}}\left(1+\beta_{\mathrm{M}}\left(\frac{\psi}{\left(\Delta^{-2}+\psi^2\right)^{1/2}}\right)^{\alpha}\right)^{-1}$$
$$=\left(1+\beta_{\mathrm{M}}\left(\frac{\psi}{\left(\Delta^{-2}+\psi^2\right)^{1/2}}\right)^{\alpha}\right)^{-1}. \quad (27)$$

Similarly, we can derive expression for $\mathcal{L}^{D}_{I^{U_L}_{\phi_{\nu,\mathrm{M}},A^c_{\mathrm{M}}}}(s)$ by applying the same approach as used for (27). Hence

$$\mathcal{L}^{D}_{I^{U_L}_{\phi_{\nu,\mathrm{M}},A^c_{\mathrm{M}}}}(s)=\left(1+\eta_1\beta_{\mathrm{M}}\left(\frac{\psi}{\left(\Delta^{-2}+\psi^2\right)^{1/2}}\right)^{\alpha}\right)^{-1}. \quad (28)$$

In (28), $\eta_1=P^{U_L}_{u,\mathrm{M}}/P^{D_L}_{\mathrm{M}}$, where $P^{U_L}_{u,\mathrm{M}}$ is the transmit power of the RU in U_L while associated with MBS, and $P^{D_L}_{\mathrm{M}}$ is the transmit power in D_L by MBS. The interference received from the other MBSs rather than the associated MBS, is random with respect to $RU_{A^c_{\mathrm{M}}}$. Therefore, we consider that the interference to $RU_{A^c_{\mathrm{M}}}$ comes from outside $B\left(x^u,R_{\circ}\left(\Delta^{-1}-\psi\right)\right)$, where x^u represents the user location outside the circular region, B, with radius $R_{\circ}\left(\Delta^{-1}-\psi\right)$. Henceforth, the LT of the interference from MBS-tier is obtained as

$$\mathcal{L}^{'}_{I^{D_L}_{\phi_{\mathrm{M}},A^c_{\mathrm{M}}}}(s)=\mathrm{E}_{I^{D_L}_{\phi_{\mathrm{M}},A^c_{\mathrm{M}}}}\left[\exp\left(-I^{D_L}_{\phi_{\mathrm{M}},A^c_{\mathrm{M}}}s\right)\right]\Big|_{s=\frac{r_z^{\alpha}\beta_{\mathrm{M}}}{P_{\mathrm{M}}^{D_L}}}$$
$$=\mathrm{E}_{I^{D_L}_{\phi_{\mathrm{M}},A^c_{\mathrm{M}}},|h_j|}\left[\exp\left(-s\sum_{j\in\phi_{\mathrm{M}}}P_{\mathrm{M}}^{D_L}|h_j|r_j^{-\alpha}\right)\right]$$
$$=\mathrm{E}_{I^{D_L}_{\phi_{\mathrm{M}},A^c_{\mathrm{M}}},|h_j|}\left[\prod_{j\in\phi_{\mathrm{M}}}\exp\left(-|h_j|\beta_{\mathrm{M}}r_{\mathrm{M}}^{\alpha}r_j^{-\alpha}\right)\right]$$
$$=\mathrm{E}_{I^{D_L}_{\phi_{\mathrm{M}},A^c_{\mathrm{M}}}}\left[\prod_{j\in\phi_{\mathrm{M}}}\mathrm{E}_{|h_j|}\exp\left(-|h_j|\beta_{\mathrm{M}}r_{\mathrm{M}}^{\alpha}r_j^{-\alpha}\right)\right]$$
$$=\mathrm{E}_{I^{D_L}_{\phi_{\mathrm{M}},A^c_{\mathrm{M}}}}\left[\prod_{j\in\phi_{\mathrm{M}}}\frac{1}{1+\beta_{\mathrm{M}}\left(\frac{r_j}{r_{\mathrm{M}}}\right)^{-\alpha}}\right]$$
$$=\exp\left(-2\pi\lambda_{\mathrm{M}}\int_{R_{\circ}\left(\Delta^{-1}-\psi\right)}^{\infty}\frac{r_j dr_j}{1+\left(\frac{r_j}{\beta_{\mathrm{M}}^{1/\alpha}\psi R_{\circ}}\right)^{\alpha}}\right)$$
$$=\exp\left(-\pi\lambda_{\mathrm{M}}\beta_{\mathrm{M}}^{2/\alpha}\psi^2R_{\circ}^2\int_{\left(\frac{R_{\circ}\left(\Delta^{-1}-\psi\right)}{\beta_{\mathrm{M}}^{1/\alpha}\psi R_{\circ}}\right)^2}^{\infty}\frac{du}{1+(u)^{\alpha/2}}\right)$$
$$=\exp\left(\frac{-\lambda_{\mathrm{M}}\pi\beta_{\mathrm{M}}\psi^{\alpha}\left(\Delta^{-1}-\psi\right)^{2-\alpha}R_{\circ}^2}{\alpha/2-1}\times\right.$$

$$ {}_2F_1\left(1, 1-2/\alpha, 2-2/\alpha, -\beta_{\mathrm{M}}\left(\frac{\psi}{\Delta^{-1}-\psi}\right)^{\alpha}\right)\Bigg). \quad (31)$$

By adopting the same approach as used for (31), we derive expression for $\mathcal{L}^{'}_{I^{U_L}_{\phi_{\nu,\mathrm{M}},A^c_{\mathrm{M}}}}(s)$ as

$$\mathcal{L}^{'}_{I^{U_L}_{\phi_{\nu,\mathrm{M}},A^c_{\mathrm{M}}}}(s) = \exp\Bigg(\frac{-\lambda_{\nu,\mathrm{M}}\pi\eta_1\beta_{\mathrm{M}}\psi^{\alpha}\left(\Delta^{-1}-\psi\right)^{2-\alpha}R_{\circ}^2}{\alpha/2-1}\times$$

$$ {}_2F_1\left(1, 1-2/\alpha, 2-2/\alpha, -\eta_1\beta_{\mathrm{M}}\left(\frac{\psi}{\Delta^{-1}-\psi}\right)^{\alpha}\right)\Bigg). \quad (32)$$

The LT of the SBS-tier is evaluated by considering the interference received from outside the circular region $B\left(x_o, R_{\circ}\left(1-\psi\right)\right)$ and it is obtained as

$$\begin{aligned}
\mathcal{L}_{I^{D_L}_{\vec{\phi}_{\mathrm{S}},A^o_{\mathrm{S}}}}(s) &= \mathrm{E}_{I^{D_L}_{\vec{\phi}_{\mathrm{S}},A^o_{\mathrm{S}}}}\left[\exp\left(-I^{D_L}_{\vec{\phi}_{\mathrm{S}},A^o_{\mathrm{S}}}s\right)\right]\Big|_{s=\frac{r_z^{\alpha}\beta_{\mathrm{M}}}{P^{D_L}_{\mathrm{M}}}} \\
&= \mathrm{E}_{I^{D_L}_{\vec{\phi}_{\mathrm{S}},A^o_{\mathrm{S}}},|h_k|}\left[\exp\left(-s\sum_{k\in\vec{\phi}_{\mathrm{S}}}P_s^{D_L}|h_k|r_k^{-\alpha}\right)\right] \\
&= \mathrm{E}_{I^{D_L}_{\vec{\phi}_{\mathrm{S}},A^o_{\mathrm{S}}},|h_k|}\left[\prod_{k\in\vec{\phi}_{\mathrm{S}}}\exp\left(-|h_k|\beta_{\mathrm{M}}\eta_2 r_{\mathrm{M}}^{\alpha}r_k^{-\alpha}\right)\right] \\
&= \mathrm{E}_{I^{D_L}_{\vec{\phi}_{\mathrm{S}},A^o_{\mathrm{S}}}}\left[\prod_{k\in\vec{\phi}_{\mathrm{S}}}\mathrm{E}_{|h_k|}\exp\left(-|h_k|\beta_{\mathrm{M}}\eta_2 r_{\mathrm{M}}^{\alpha}r_k^{-\alpha}\right)\right] \\
&= \mathrm{E}_{I^{D_L}_{\vec{\phi}_{\mathrm{S}},A^o_{\mathrm{S}}}}\left[\prod_{k\in\vec{\phi}_{\mathrm{S}}}\frac{1}{1+\beta_{\mathrm{M}}\eta_2\left(\frac{r_k}{r_{\mathrm{M}}}\right)^{-\alpha}}\right] \\
&= \exp\left(-2\pi\vec{\lambda}_{\mathrm{S}}\int_{R_{\circ}(1-\psi)}^{\infty}\frac{r_k dr_k}{1+\left(\frac{r_k}{\left(\eta_2\beta_{\mathrm{M}}\right)^{1/\alpha}\psi R_{\circ}}\right)^{\alpha}}\right) \\
&= \exp\left(-\pi\vec{\lambda}_{\mathrm{S}}\left(\eta_2\beta_{\mathrm{M}}\right)^{2/\alpha}\psi^2R_{\circ}^2\int_{\left(\frac{R_{\circ}(1-\psi)}{\left(\eta_2\beta_{\mathrm{M}}\right)^{1/\alpha}\psi R_{\circ}}\right)^2}^{\infty}\frac{du}{1+(u)^{\alpha/2}}\right) \\
&= \exp\Bigg(\frac{-\vec{\lambda}_{\mathrm{S}}\pi\eta_2\beta_{\mathrm{M}}\psi^{\alpha}\left(1-\psi\right)^{2-\alpha}R_{\circ}^2}{\alpha/2-1}\times \\
&\quad {}_2F_1\left(1, 1-2/\alpha, 2-2/\alpha, -\beta_{\mathrm{M}}\eta_2\left(\frac{\psi}{1-\psi}\right)^{\alpha}\right)\Bigg). \quad (33)
\end{aligned}$$

Here, $\eta_2 = P_{\mathrm{S}}^{D_L}/P_{\mathrm{M}}^{D_L}$, where $P_{\mathrm{S}}^{D_L}$ is the power transmitted by SBS in D_L.

Following the same approach as used in (33), the expression for $\mathcal{L}_{I^{U_L}_{\vec{\phi}_{\nu,\mathrm{S}},A^o_{\mathrm{S}}}}(s)$ can be obtained as

$$\begin{aligned}
\mathcal{L}_{I^{U_L}_{\vec{\phi}_{\nu,\mathrm{S}},A^o_{\mathrm{S}}}}(s) &= \exp\Bigg(\frac{-\vec{\lambda}_{\nu,\mathrm{S}}\pi\eta_3\beta_{\mathrm{M}}\psi^{\alpha}\left(1-\psi\right)^{2-\alpha}R_{\circ}^2}{\alpha/2-1} \\
&\quad \times {}_2F_1\left(1, 1-2/\alpha, 2-2/\alpha, -\beta_{\mathrm{M}}\eta_3\left(\frac{\psi}{1-\psi}\right)^{\alpha}\right)\Bigg). \quad (34)
\end{aligned}$$

The expression in (25) requires averaging over r_{M} and $R_{\circ}$. The marginal PDF of ψ, i.e., $f_{\psi}\left(\psi\right)$, can now be evaluated by taking the average over $R_{\circ}$ and ψ, and by substituting $r_{\mathrm{M}} = \psi R_{\circ}$ as

$$\begin{aligned}
f_{\psi}\left(\psi\right) &= \int_{-\infty}^{\infty}|R_{\circ}|f_{R_{\circ},r_{\mathrm{M}}}\left(R_{\circ},\psi R_{\circ}\right)dR_{\circ} \\
&= \int_0^{\infty}R_{\circ}\times 2\pi\lambda_{\mathrm{M}}R_s\Delta^{-2}\exp\Big(-\pi\lambda_{\mathrm{M}}\left(R_s/\Delta\right)^2\Big) \\
&\quad \times 2\pi\lambda_{\mathrm{M}}\psi R_s\exp\Big(-\pi\lambda_{\mathrm{M}}\left(\psi R_s\right)^2\Big)dR_{\circ} \\
&= 2\Delta^{-2}\psi\left(\Delta^{-2}+\psi^2\right)^{-2}. \quad (37)
\end{aligned}$$

The probability that the MBS associated RU, located in A^c_{M}, is given as $p_{A^c_{\mathrm{M}}} = P\left(x^o \in B\left(0, R_{\circ}\right)\right) \approx P\left(\psi < 1\right)$. Therefore, the PDF in (37) can be used to calculate $p_{A^c_{\mathrm{M}}}$ as

$$p_{A^c_{\mathrm{M}}} = \int_0^1 f_{\psi}\left(\psi\right)d\psi = \left(1+\Delta^{-2}\right)^{-1}, \quad (38)$$

and

$$p_{A^o_{\mathrm{M}}} = \left(1-p_{A^c_{\mathrm{M}}}\right) = \left(1+\Delta^{2}\right)^{-1}. \quad (39)$$

The coverage probability expression of SFR-enabled Stienen's cell based SBS deployment for MBS associated RU in A^o_{M} with SFR, $P^{cov}_{A^c_{\mathrm{M}},\varrho}\left(\beta_{\mathrm{M}}\right)$, can be written as

$$\begin{aligned}
P^{cov*}_{A^c_{\mathrm{M}},\varrho}\left(\beta_{\mathrm{M}}\right) &= \frac{1}{p_{A^c_{\mathrm{M}}}}\int_0^1\int_0^{\infty}\Bigg(\mathcal{L}^{D}_{I^{D_L}_{\phi_{\mathrm{M}},A^c_{\mathrm{M}}}}\times\mathcal{L}^{D}_{I^{U_L}_{\phi_{\nu,\mathrm{M}},A^c_{\mathrm{M}}}}\times\mathcal{L}^{'}_{I^{D_L}_{\phi_{\mathrm{M}},A^c_{\mathrm{M}}}} \\
&\quad \times\mathcal{L}^{'}_{I^{U_L}_{\phi_{\nu,\mathrm{M}},A^c_{\mathrm{M}}}}\times\mathcal{L}_{I^{D_L}_{\vec{\phi}_{\mathrm{S}},A^o_{\mathrm{S}}}}\times\mathcal{L}_{I^{U_L}_{\vec{\phi}_{\nu,\mathrm{S}},A^o_{\mathrm{S}}}}\Bigg)f_{R_{\circ}}\left(R_{\circ}\right)f_{\psi}\left(\psi\right)dR_{\circ}d\psi. \quad (40)
\end{aligned}$$

By substituting (1), (27), (28), (31), (32), (33), (34), (37) and (38) into (40), we obtain $P^{cov}_{A^c_{\mathrm{M}},\varrho}\left(\beta_{\mathrm{M}}\right)$ as (29).

2) Coverage probability of SFR-enabled Stienen's cell based SBS deployment for MBS-AU in A^o_M: The coverage probability expression of SFR-enabled Stienen's cell based SBS deployment for MBS associated RU in A^o_{M}, $P^{cov}_{A^o_{\mathrm{M}},\varrho}\left(\beta_{\mathrm{M}}\right)$, is given as

$$\begin{aligned}
P^{cov*}_{A^o_{\mathrm{M}},\varrho}\left(\beta_{\mathrm{M}}\right) &= \frac{1}{\left(1-p_{A^c_{\mathrm{M}}}\right)}\int_1^{\infty}\int_0^{\infty}\Bigg(\mathcal{L}^{D}_{I^{D_L}_{\phi_{\mathrm{M}},A^c_{\mathrm{M}}}}\times\mathcal{L}^{D}_{I^{U_L}_{\phi_{\nu,\mathrm{M}},A^c_{\mathrm{M}}}}\times\mathcal{L}^{'}_{I^{D_L}_{\phi_{\mathrm{M}},A^c_{\mathrm{M}}}} \\
&\quad \times\mathcal{L}^{'}_{I^{U_L}_{\phi_{\nu,\mathrm{M}},A^c_{\mathrm{M}}}}\times\mathcal{L}_{I^{D_L}_{\vec{\phi}_{\mathrm{S}},A^o_{\mathrm{S}}}}\times\mathcal{L}_{I^{U_L}_{\vec{\phi}_{\nu,\mathrm{S}},A^o_{\mathrm{S}}}}\Bigg)f_{R_{\circ}}(R_{\circ})f_{\psi}\left(\psi\right)dR_{\circ}d\psi. \quad (41)
\end{aligned}$$

Moreover, based on the similar approach as used for (29), (30) can be obtained from (41).

D. Coverage Probability for Stienen's Cell based SBS Deployment without SFR

Lastly, similar to the procedure for deriving (29) and (30), the coverage probability expressions of Stienen's cell based SBS deployment without SFR for MBS associated RU in A^c_{M} and A^o_{M}, i.e., $P^{cov}_{A^c_{\mathrm{M}},\varrho}\left(\beta_{\mathrm{M}}\right)$, and $P^{cov}_{A^o_{\mathrm{M}},\varrho}\left(\beta_{\mathrm{M}}\right)$, are given as (35) and (36), respectively.

$$P^{cov}_{A^c_{\mathrm{M}},\varrho}(\beta_{\mathrm{M}})=\int_0^1 \frac{2\psi\left(1+\Delta^{-2}\right)}{\Delta^2\left(\Delta^{-2}+\psi^2\right)^2}\left(1+\beta_{\mathrm{M}}\left(\frac{\psi}{\left(\Delta^{-2}+\psi^2\right)^{1/2}}\right)^{\alpha}\right)^{-2}\left(1+\eta_1\beta_{\mathrm{M}}\left(\frac{\psi}{\left(\Delta^{-2}+\psi^2\right)^{1/2}}\right)^{\alpha}\right)^{-2}$$
$$\left(1+\frac{\beta_{\mathrm{M}}\Delta^2\psi^{\alpha}}{\alpha/2-1}\left[\left(\Delta^{-1}-\psi\right)^{2-\alpha}\left(\mathcal{J}\left(\alpha,-\beta_{\mathrm{M}}\left(\frac{\psi}{\left(\Delta^{-1}-\psi\right)}\right)^{\alpha}\right)+\frac{\eta_1\lambda_{\nu,\mathrm{M}}}{\lambda_{\mathrm{M}}}\mathcal{J}\left(\alpha,-\eta_1\beta_{\mathrm{M}}\left(\frac{\psi}{\left(\Delta^{-1}-\psi\right)}\right)^{\alpha}\right)\right)\right.\right.$$
$$\left.\left.+\frac{(1-\psi)^{2-\alpha}}{\lambda_{\mathrm{M}}}\left(\vec{\lambda}_{\mathrm{S}}\eta_2\mathcal{J}\left(\alpha,-\eta_2\beta_{\mathrm{M}}\left(\frac{\psi}{(1-\psi)}\right)^{\alpha}\right)+\vec{\lambda}_{\nu,\mathrm{S}}\eta_3\mathcal{J}\left(\alpha,-\eta_3\beta_{\mathrm{M}}\left(\frac{\psi}{(1-\psi)}\right)^{\alpha}\right)\right)\right]\right)^{-1}d\psi. \quad (35)$$

$$P^{cov}_{A^o_{\mathrm{M}},\varrho}(\beta_{\mathrm{M}})=\int_1^{\infty} \frac{2\psi\left(1+\Delta^{-2}\right)}{\left(\Delta^{-2}+\psi^2\right)^2}\left(1+\beta_{\mathrm{M}}\left(\frac{\psi}{\left(\Delta^{-2}+\psi^2\right)^{1/2}}\right)^{\alpha}\right)^{-2}\left(1+\eta_1\beta_{\mathrm{M}}\left(\frac{\psi}{\left(\Delta^{-2}+\psi^2\right)^{1/2}}\right)^{\alpha}\right)^{-2}$$
$$\left(1+\frac{\beta_{\mathrm{M}}\Delta^2\psi^{\alpha}}{\alpha/2-1}\left[\left(\Delta^{-1}-\psi\right)^{2-\alpha}\left(\mathcal{J}\left(\alpha,-\beta_{\mathrm{M}}\left(\frac{\psi}{\left(\Delta^{-1}-\psi\right)}\right)^{\alpha}\right)+\frac{\eta_1\lambda_{\nu,\mathrm{M}}}{\lambda_{\mathrm{M}}}\mathcal{J}\left(\alpha,-\eta_1\beta_{\mathrm{M}}\left(\frac{\psi}{\left(\Delta^{-1}-\psi\right)}\right)^{\alpha}\right)\right)\right.\right.$$
$$\left.\left.+\frac{(1-\psi)^{2-\alpha}}{\lambda_{\mathrm{M}}}\left(\vec{\lambda}_{\mathrm{S}}\eta_2\mathcal{J}\left(\alpha,-\eta_2\beta_{\mathrm{M}}\left(\frac{\psi}{(1-\psi)}\right)^{\alpha}\right)+\vec{\lambda}_{\nu,\mathrm{S}}\eta_3\mathcal{J}\left(\alpha,-\eta_3\beta_{\mathrm{M}}\left(\frac{\psi}{(1-\psi)}\right)^{\alpha}\right)\right)\right]\right)^{-1}d\psi. \quad (36)$$

TABLE III: Simulation parameters

Parameter	Configuration
Channel bandwidth	10 MHz
SBS deployment	PPP and PHP
User and MBS deployment	PPP
$\lambda_{\mathrm{S}}/\lambda_{\mathrm{M}}$	(15, 35, 80, and 200) / (1 km^2)
$\vec{\lambda}_{\mathrm{S}}/\lambda_{\mathrm{M}}$	$\approx (0.5\lambda_{\mathrm{S}}/\lambda_{\mathrm{M}})$ / (1 km^2)
Δ	1/2
$\lambda_{\nu,\mathrm{S}}$, $\lambda_{\nu,\mathrm{M}}$	$\lambda_{\mathrm{S}}/\lambda_{\mathrm{M}}$ / (1 km^2) each
$P_{\nu}, P_{\mathrm{S}}, P_{\mathrm{M}}$	10 dBm, 20 dBm, and 40 dBm, respectively
$\alpha_m = \alpha_s = \alpha$	$2 < \alpha \leq 4$

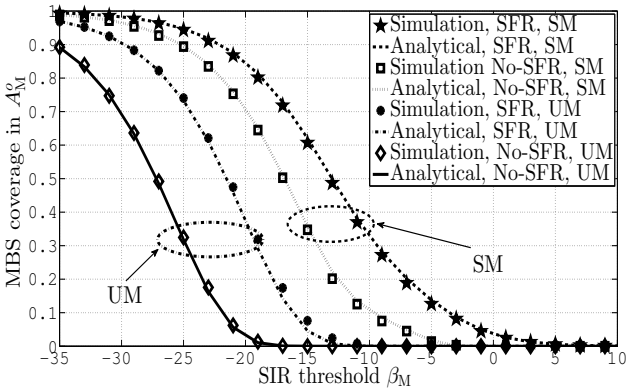

Fig. 3: MBS coverage in A^o_{M} versus SIR threshold β_{M} as expressed in (13), (20), (30) and (36).

IV. Numerical Results and Discussions

In this section, we provide analytical and simulation results for the proposed framework. The section is further divided into two subsections, i.e., (i) MBS edge user coverage versus SIR threshold, and (ii) MBS edge user coverage versus densities of MBSs, SBSs, MBS-AUs, and SBS-AUs. Mathematica 11 and MATLAB 2017B have been used to derive the coverage probability expressions and perform simulations. The network configuration parameters are listed in Tab. III.

A. MBS Edge User Coverage versus SIR Threshold

We evaluate first MBS edge user coverage versus SIR threshold for different network scenarios, such as with and without Stienen's cell based SBS deployment, with and without SFR employment, and coverages in A^c_{M} and A^o_{M}.

Fig. 3 evaluates the coverage probability for both uniform SBS deployment model (denoted as UM in the plots) and Stienen's cell based SBS deployment model (denoted as SM in the plots) considering different values of β_{M}. Moreover, the results are obtained by considering with and without SFR employment, and by using (13), (20), (30) and (36). The plots in the figure show that, across various SIR thresholds, significant D_L coverage improvement has been achieved by Stienen's cell based SBS deployment model along with SFR compared with uniform SBS deployment. When β_{M} = -15 dB, for instance, a 49% improvement has been observed. This benefit is achieved since few SBSs are required based on Stienen's model. Furthermore, the figure indicates significant interference abating while using SFR against the No-SFR scenario. This performance gain introduced by SFR is achieved thanks to its efficient resource distribution (see Tab. II) as compared with No-SFR [1], [15]. More specifically, in the No-SFR case, all spectrum in the same frequency band is available to and shared by both MBSs and SBSs, leading to severe co-channel interference especially for ultra-dense HetNets. Through SFR, on the other hand, MBSs and SBSs are assigned different bands in a multi-region environment and, thus, it causes less network interference. Here, uniform HetNet with No-SFR scenario leads to lowest edge user coverage.

Similarly, the plots in Fig. 4 demonstrate the MBS coverage probability for different values of β_{M} and $\lambda_{\mathrm{S}}/\lambda_{\mathrm{M}}$ in accordance with (30) and (36). The figure shows that an increase in the value of $\lambda_{\mathrm{S}}/\lambda_{\mathrm{M}}$ degrades MBS coverage due to interference escalation. The result further reveals that Stienen's cell based

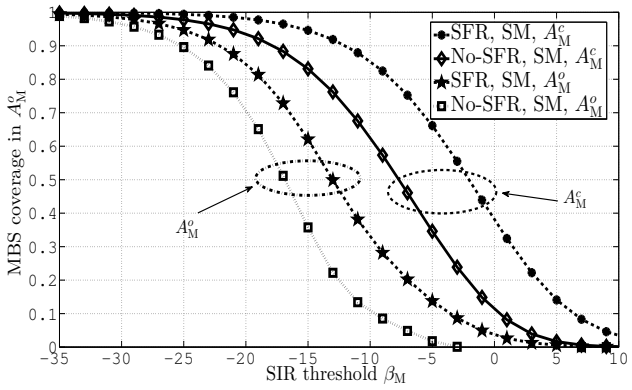

Fig. 4: MBS coverage in A^o_M versus SIR threshold β_M as expressed in (13), (20), (30) and (36).

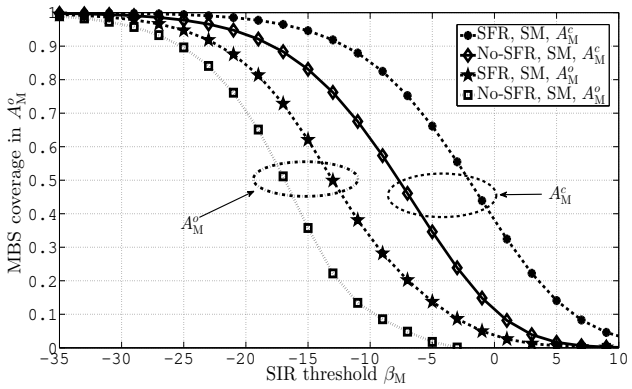

Fig. 5: MBS coverage in A^o_M versus SIR threshold β_M as expressed in (29), (30), (35), and (36). Herein, we configure $\lambda_S/\lambda_M = 80$.

SBS deployment with $\lambda_S/\lambda_M = 80$ surpasses the other scenarios. This is due to the fact that Stienen's deployment diminishes network interference because of a smaller number of deployed SBSs.

Morever, we compare the MBS coverage probability against different values of β_M for the RU located in A^c_M and A^o_M in Fig. 5. This figure illustrates the coverage probabilities for Stienen's cell based SBS deployment with and without SFR employment as expressed in (29), (30), (35) and (36). It can be observed that the RU located in A^c_M experiences enhanced coverage probability due to its closeness with MBS as compared with an RU in A^o_M. Furthermore, SFR-enabled Stienen's cell based SBS deployment for $\lambda_S/\lambda_M = 80$ surpasses the other scenarios. This is due to effective resource allocation by SFR and lower interference caused by Stienen's model based SBS deployment.

B. MBS Edge User Coverage versus Densities of MBSs, SBSs, MBS-AUs, and SBS-AUs

Next, we present the MBS edge user coverage with different densities of MBSs, SBSs, MBS-AUs, and SBS-AUs. The results for different network scenarios are given below.

In Fig. 6, we present coverage probabilities as, λ_S/λ_M, and $\vec{\lambda}_S/\lambda_M$ vary, in conjunction with different network layout

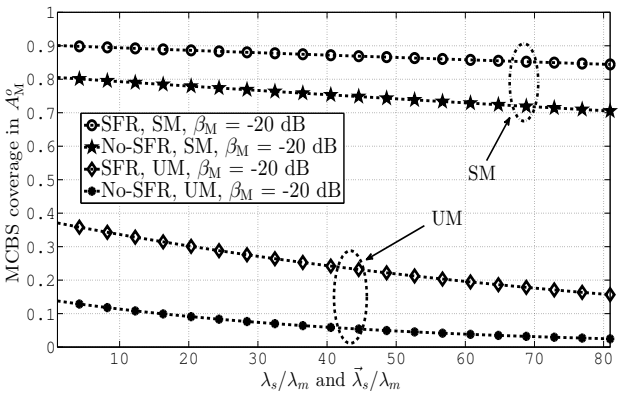

Fig. 6: MBS coverage in A^o_M versus different values of λ_S/λ_M and $\vec{\lambda}_S/\lambda_M$ as expressed in (13), (20), (30) and (36).

scenarios by configuring β_M = -20 dB, $\lambda_S/\lambda_M = 0$ to 80, and $\vec{\lambda}_S/\lambda_M = 0$ to 80 respectively. Here, $\lambda_{\nu,S}$ and $\lambda_{\nu,M}$ are configured to be 80. The results are obtained in accordance with (13), (20), (30), and (36). The plots demonstrate that a higher density of SBSs in an MBS coverage area leads to lower coverage probabilities in all the scenarios due to a higher number of user associations with SBSs. Moreover, the figure shows that SFR-enabled Stienen's cell based SBS employment outperforms the other simulation scenarios. Therefore, SBS distribution via PHP leads to significant improvement for ICI and MBS-I mitigation, as compared with PPP based SBS distribution.

Similarly, we illustrate in Fig. 7 the achieved coverage probabilities with different values of SBS density, $\vec{\lambda}_S/\lambda_M$, which are expressed in (29) and (30). For this particular setup, the results are obtained for an RU located both in A^c_M and A^o_M with β_M = -5 dB, -10 dB and -15 dB respectively. The figure shows that the RU experiences better coverage in A^c_M, thanks to its close MBS proximity as compared with A^o_M. Moreover, higher values of β_M give rise to lower coverage probabilities in both A^c_M and A^o_M due to fewer user associations with MBS. Here, it can be observed that the coverage of MBS edge users decreases with the increase of SBS density as more users are associated with SBSs. Furthermore, this result depicts that higher SBS density leads to higher network interference due to the increase in network congestion.

In Fig. 8, we demonstrate the coverage probabilities with different values of SBS-AUs density, $\vec{\lambda}_{\nu,S}$, in A^o_M. This figure considers: (i) SFR-enabled Stienen's cell based SBS deployment, and (ii) No-SFR with Stienen's cell based SBS deployment, for different values of $\vec{\lambda}_S/\lambda_M$ where β_M is configured as β_M = -20 dB, -15 dB, -10 dB, and -5 dB respectively. Clearly, the results are in line with the derived expressions in (29) and (30). The results demonstrate that increased values of $\vec{\lambda}_{\nu,S}$ lead to reduced coverage due to significant interference. It can also be noticed that β_M = -20 dB improves the network coverage against β_M = -15 dB, -10 dB, and -5 dB as a higher number of users get associated with the BS.

In Fig. 9, the MBS coverages in A^c_M and A^o_M, as expressed in (29) and (30), are compared with each other for different values of λ_M. The results are obtained for β_M = -15 dB,

This article has been accepted for publication in a future issue of this journal, but has not been fully edited. Content may change prior to final publication. Citation information: DOI 10.1109/TVT.2020.3048090, IEEE Transactions on Vehicular Technology

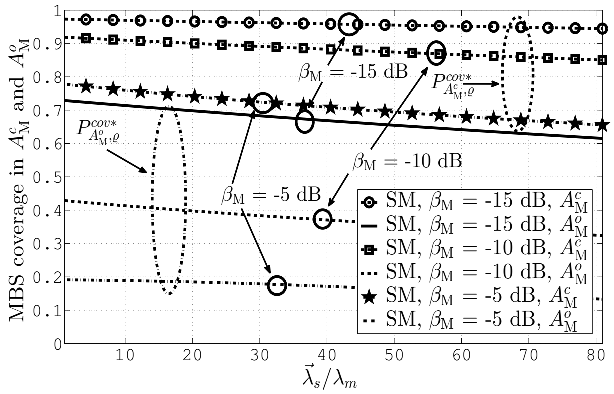

Fig. 7: MBS coverage in A_{M}^{c}, and in A_{M}^{o}, as expressed in (29) and (30).

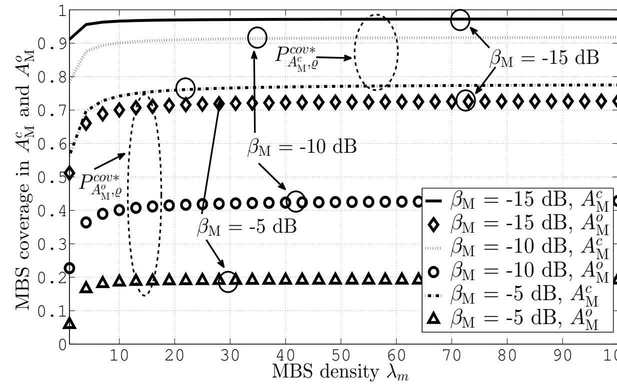

Fig. 9: MBS coverage in A_{M}^{c}, and in A_{M}^{o}, as expressed in (29) and (30).

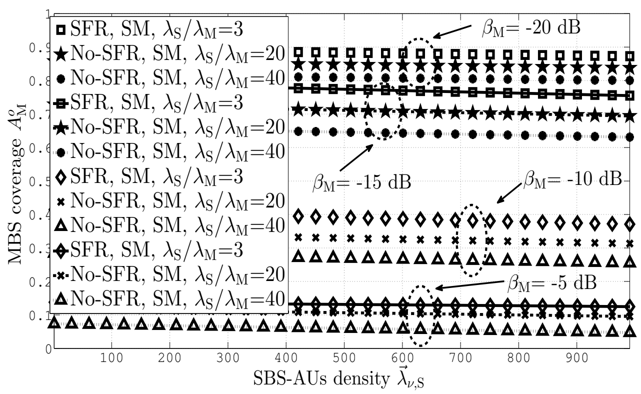

Fig. 8: MBS coverage in A_{M}^{o} versus SBS-AUs density, in A_{M}^{o}, as expressed in (30) and (36).

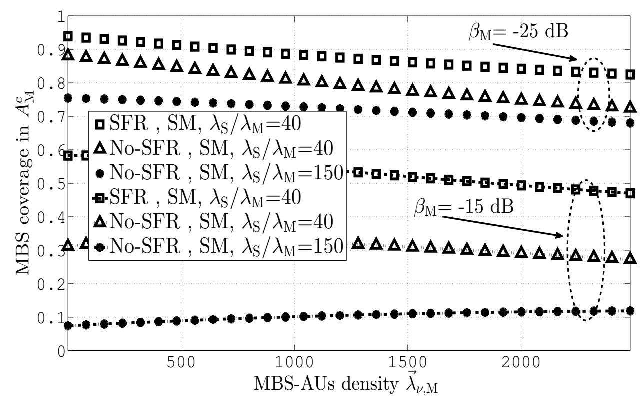

Fig. 10: MBS coverage in A_{M}^{o} versus MBS-AUs density in A_{M}^{c}, as expressed in (30) and (36).

-10 dB, and -5 dB. The results demonstrate that the *RU* experiences enhanced MBS coverage in A_{M}^{c} due to its close MBS proximity as compared with when it is located in A_{M}^{o}. Moreover, a lower value of β_{M} leads to enhanced MBS coverage, thanks to more MBS user associations. Furthermore, this figure reveals that higher MBS density does not increase the network coverage significantly due to higher ICI and MBS-I.

Finally, in Fig. 10, we present the coverage probabilities with $\lambda_{\nu,\mathrm{M}}$, in A_{M}^{c} and A_{M}^{o}. The results are obtained for: (i) SFR-enabled Stienen's cell based SBS deployment, and (ii) No-SFR with Stienen's cell based SBS deployment, as expressed in (30) and (36), respectively, with different values of $\lambda_{\mathrm{S}}/\lambda_{\mathrm{M}}$. Moreover, the results are derived for β_{M} = -25 dB and -15 dB. It can be observed that higher values of $\lambda_{\nu,\mathrm{M}}$ lead to lower coverage because of increased network interference. It can also be noticed that β_{M} = -25 dB improves coverage performance as compared with β_{M} = -15 dB as a result of more user associations. Furthermore, the *RU* experiences better coverage in A_{M}^{c} owing to its close MBS proximity as compared with an *RU* in A_{M}^{o}. The concave nature in the lower plots at β = -15 dB implies that there are optimum values of MBS-AUs' density in the network. An optimum MBS-AUs' density indicates highest coverage. Below and above this optimum MBS-AUs' density, the coverage will degrade. This is again due to the fact that a lower number of users are associated with MBS.

V. Conclusions and Future Work

In this paper, we have proposed a novel cell deployment strategy that combines Stienen's model with SFR. The proposed strategy is evaluated considering PPP and PHP SBS deployment for with and without SFR employment cases. Focusing on MBS coverage, the analysis is performed on a reference user located inside and outside Stienen's cell. The expressions for coverage probabilities under plausible scenarios are derived and validated through simulations. The results indicate that Stienen's cell based SBS deployment along with SFR leads to much better coverage for MBS edge users in contrast to uniform SBS deployment. Moreover, the coverage is improved for the reference user located inside Stienen's cell as compared with the one located outside of Stienen's cell. The results also demonstrate that with higher densities of MBSs, SBSs, MBS-AUs, and SBS-AUs, the network performance is reduced due to increased interference. As a promising direction for our work, we will extend our analysis to more than two-tiers of BSs. How many tiers will be included in our model depends on the added complexity of the to-be-developed model.

APPENDIX A
PROOF OF STEP (2) IN (8)

Proof : Based on [5] and [11], we further obtain $P^{cov*}_{A^c_z,\zeta}(\beta_z)$ as

$$P^{cov*}_{A^c_z,\zeta}(\beta_z) = P\left(\frac{P_z^{D_L}|h_z|r_z{}^{-\alpha}}{I^{D_L}_{\phi_z,A^c_z}+I^{U_L}_{\phi_{\nu,z},A^c_z}+I^{D_L}_{\phi_\tau,A^o_\tau}+I^{U_L}_{\phi_{\nu,\tau},A^o_\tau}} > \beta_z\right). \quad (42)$$

By keeping $|h_z|$ on one side of the inequality and moving the rest of the parameters to the other side, we transform (42) as

$$P^{cov*}_{A^c_z,\zeta}(\beta_z) = P\left(|h_z| > \frac{r_z^\alpha \beta_z}{P_z^{D_L}}\left(I^{D_L}_{\phi_z,A^c_z}+I^{U_L}_{\phi_{\nu,z},A^c_z}+I^{D_L}_{\phi_\tau,A^o_\tau}+I^{U_L}_{\phi_{\nu,\tau},A^o_\tau}\right)\right). \quad (43)$$

Now, following a similar derivation procedure presented on pages 14-16 in [11], (43) transforms into the expression of Step (2) in (8).

REFERENCES

[1] M. S. Haroon, Z. H. Abbas, G. Abbas, and F. Muhammad, "Analysis of interference mitigation in heterogeneous cellular networks using soft frequency reuse and load balancing," in *Proc. IEEE ITNAC*, Nov. 2018, pp. 1–6.

[2] A. Ullah, Z. H. Abbas, G. Abbas, F. Muhammad, and L. Jiao, "Performance analysis of user-centric SBS deployment with load balancing in heterogeneous cellular networks: A Thomas cluster process approach," *Comput. Netw.*, vol. 170, p. 107120, Mar. 2020.

[3] H. Zhang, C. Jiang, R. Q. Hu, and Y. Qian, "Self-organization in disaster-resilient heterogeneous small cell networks," *IEEE Netw.*, vol. 30, no. 2, pp. 116–121, Mar. 2016.

[4] H. ElSawy, E. Hossain, and M. Haenggi, "Stochastic geometry for modeling, analysis, and design of multi-tier and cognitive cellular wireless networks: A survey," *IEEE Commun. Surveys Tuts.*, vol. 15, no. 3, pp. 996–1019, Jun. 2013.

[5] F. Muhammad, Z. H. Abbas, and F. Y. Li, "Cell association with load balancing in nonuniform heterogeneous cellular networks: Coverage probability and rate analysis," *IEEE Trans. Veh. Technol.*, vol. 66, no. 6, pp. 5241–5255, Sep. 2017.

[6] M. Makhanbet, T. Lv, M. Orynbet, and B. Suleimenov, "A fully distributed and clustered learning of power control in user-centric ultra-dense HetNets," *IEEE Trans. Veh. Technol.*, vol. 69, no. 10, pp. 11 529–11 543, Oct. 2020.

[7] S. Faruque, *Radio Frequency Multiple Access Techniques Made Easy*. Springer, 2019.

[8] Z. H. Abbas, F. Muhammad, and L. Jiao, "Analysis of load balancing and interference management in heterogeneous cellular networks," *IEEE Access*, vol. 5, pp. 14 690–14 705, Jul. 2017.

[9] S. Ni, J. Zhao, H. H. Yang, and Y. Gong, "Enhancing downlink transmission in MIMO HetNet with wireless backhaul," *IEEE Trans. Veh. Technol.*, vol. 68, no. 7, pp. 6817–6832, May 2019.

[10] Z. H. Abbas, M. S. Haroon, G. Abbas, and F. Muhammad, "SIR analysis for non-uniform HetNets with joint decoupled association and interference management," *Comput. Commun.*, vol. 155, pp. 48–57, Apr. 2020.

[11] B. Błaszczyszyn, M. Haenggi, P. Keeler, and S. Mukherjee, *Stochastic Geometry Analysis of Cellular Networks*. Cambridge University Press, 2018.

[12] B. U. Kazi and G. Wainer, "Coordinated multi-cell cooperation with user centric dynamic coordination station," *Comput. Netw.*, vol. 166, p. 106948, Jan. 2020.

[13] P. Deb, A. Mukherjee, and D. De, "Fractional frequency reuse based frequency allocation for 5G HetNet using master–slave algorithm," *Physical Commun.*, vol. 42, p. 101158, 2020.

[14] L. Guo, S. Cong, and Z. Sun, "Multichannel analysis of soft frequency reuse and user association in two-tier heterogeneous cellular networks," *EURASIP J. Wireless Commun. and Netw.*, vol. 2017, no. 1, pp. 1–20, Dec. 2017.

[15] M. S. Haroon, Z. H. Abbas, G. Abbas, and F. Muhammad, "Coverage analysis of ultra-dense heterogeneous cellular networks with interference management," *Wireless Netw.*, pp. 1–13, Apr. 2019.

[16] H. B. Nafea, E. M. Soultan, and F. W. Zaki, "Availability of cellular systems based on space domain," *Wireless Pers. Commun.*, vol. 107, no. 4, pp. 1881–1910, 2019.

[17] Z. H. Abbas, G. Abbas, M. S. Haroon, F. Muhammad, and S. Kim, "Proactive uplink interference mitigation in HetNets stressed by uniformly distributed wideband jammers," *Electron.*, vol. 8, no. 12, p. 1496, Dec. 2019.

[18] R. Hernandez-Aquino, S. A. R. Zaidi, M. Ghogho, D. McLernon, and A. Swami, "Stochastic geometric modeling and analysis of non-uniform two-tier networks: A Stienen's model-based approach," *IEEE Trans. Wireless Commun.*, vol. 16, no. 6, pp. 3476–3491, Mar. 2017.

[19] R. Hernandez-Aquino, S. A. R. Zaidi, D. McLernon, and M. Ghogho, "Modelling and performance evaluation of non-uniform two-tier cellular networks through Stienen model," in *Proc. IEEE ICC*, May 2016, pp. 1–6.

[20] M. S. Haroon, Z. H. Abbas, F. Muhammad, and G. Abbas, "Analysis of coverage-oriented small base station deployment in heterogeneous cellular networks," *Physical Commun.*, vol. 38, p. 100908, Feb. 2020.

[21] U. S. Hashmi, S. A. R. Zaidi, A. Imran, and A. Abu-Dayya, "Enhancing downlink QoS and energy efficiency through a user-centric Stienen cell architecture for mmWave networks," *IEEE Trans. Green Commun. Netw.*, vol. 4, no. 2, pp. 387–403, 2020.

[22] A. Afzal, S. A. R. Zaidi, D. McLernon, M. Ghogho, and A. Feki, "M2M meets D2D: Harnessing D2D interfaces for the aggregation of M2M data," in *IEEE ICC*. IEEE, 2017, pp. 1–6.

[23] E. M. Soultan, H. B. Nafea, and F. W. Zaki, "Interference management for different 5G cellular network constructions," *Wireless Pers. Commun.*, pp. 1–20, 2020.

[24] M. Fereydooni, M. Sabaei, M. Dehghan, G. B. Eslamlou, and M. Rupp, "Analytical evaluation of heterogeneous cellular networks under flexible user association and frequency reuse," *Comput. Commun.*, vol. 116, pp. 147–158, Jan. 2018.

[25] H. Wu, Z. Wei, Y. Hou, N. Zhang, and X. Tao, "Cell-edge user offloading via flying UAV in non-uniform heterogeneous cellular networks," *IEEE Trans. Wireless Commun.*, vol. 19, no. 4, pp. 2411–2426, Apr. 2020.

[26] Z. H. Abbas, G. Abbas, M. S. Haroon, and F. Muhammad, "Analysis of interference management in heterogeneous cellular networks in the presence of wideband jammers," *IEEE Commun. Lett.*, vol. 24, no. 5, pp. 1138–1141, 2020.

[27] X. Jia, Q. Fan, W. Xu, and L. Yang, "Cross-tier dual-connectivity designs of three-tier HetNets with decoupled uplink/downlink and global coverage performance evaluation," *IEEE Access*, vol. 7, pp. 16 816–16 836, 2019.

[28] 3GPP-TR-38.913, "5G; study on scenarios and requirements for next generation access technologies," v14.3.0, R14, May 2017.

[29] Y. Liu, F. R. Yu, X. Li, H. Ji, and V. C. Leung, "Distributed self-optimizing interference management in ultra-dense networks with non-orthogonal multiple access," *Wireless Netw.*, pp. 1–15, 2020.

[30] J. G. Andrews, S. Buzzi, W. Choi, S. V. Hanly, A. Lozano, A. C. Soong, and J. C. Zhang, "What will 5G be?" *IEEE J. Sel. Areas Commun.*, vol. 32, no. 6, pp. 1065–1082, Jun. 2014.

[31] C. Saha and H. S. Dhillon, "Load on the typical Poisson Voronoi cell with clustered user distribution," *IEEE Wireless Commun. Lett.*, vol. 9, no. 9, pp. 1361–1365, Sep. 2020.

[32] D. O. Morley and M. Wilson, "Voronoi diagrams in quasi-2D hard sphere systems," *J. Statistical Mechanics: Theory and Experiment*, vol. 2020, no. 9, p. 093201, Sep. 2020.

[33] K. Shehzad, N. M. Khan, and J. Ahmed, "Performance analysis of coverage-centric heterogeneous cellular networks using dual-slope path loss model," *Comput. Netw.*, p. 107672, Article in press, Nov. 2020.

[34] U. S. Hashmi, *Novel User-centric Architectures for Future Generation Cellular Networks: Design, Analysis and Performance Optimization*. University of Oklahoma Press, 2019.

[35] F. Muhammad, Z. H. Abbas, and L. Jiao, "Analysis of interference avoidance with load balancing in heterogeneous cellular networks," in *Proc. IEEE PIMRC*, Sep. 2016, pp. 1–6.

Ziaul Haq Abbas received the M.Phil. degree in electronics from Quaid-e-Azam University, Pakistan, in 2001, and the Ph.D. degree from the Agder Mobility Laboratory, Department of Information and Communication Technology, University of Agder, Norway, in 2012. He joined the Ghulam Ishaq Khan (GIK) Institute of Engineering Sciences and Technology, Pakistan. In 2012, he was a Visiting Researcher with the Department of Electrical and Computer Engineering, University of Minnesota, USA. He is currently an Associate Professor with the Faculty of Electrical Engineering and a co-founding member of the Telecommunications and Networking (TeleCoN) Research Lab at GIK Institute. His research interests include energy efficiency in hybrid mobile and wireless communication networks, 4G and beyond mobile systems, mesh and ad hoc networks, traffic engineering in wireless networks, performance evaluation of communication protocols and networks by analysis and simulation, quality-of-service in wireless networks, green wireless communication, and cognitive radio.

Muhammad Sajid Haroon received the B.Sc. degree in electronics engineering from International Islamic University Islamabad, Pakistan, in 2007, M.S. degrees in electrical engineering from COMSATS Institute of Information Technology, Attock, Pakistan, in 2013, and Ph.D. degree from Ghulam Ishaq Khan Institute of Engineering Science and Technology, Swabi, Pakistan. He is currently a post-doc researcher at Hanyang University, Ansan, South Korea. His research interests include interference mitigation in cellular networks, next generations cellular networks, stochastic processes and digital signal processing.

Fazal Muhammad received the B.Sc. and M.Sc. degrees in electrical engineering from the University of Engineering and Technology, Peshawar, Pakistan, in 2004 and 2007, respectively, and the Ph.D. degree in electronic engineering from GIK Institute of Engineering Sciences and Technology, Pakistan in 2017. He is currently working as Assistant Professor and Head of Electrical Engineering Department at City University of Sciences and Information Technology, Peshawar. He is the Secretary of Institutions of Engineers, Pakistan, Peshawar Centre. His research interests include heterogeneous cellular networks, cognitive radio networks, and sensor networks.

Ghulam Abbas received the B.S. degree in computer science from University of Peshawar, Pakistan, in 2003, and the M.S. degree in distributed systems and the Ph.D. degree in computer networks from the University of Liverpool, U.K., in 2005 and 2010, respectively. From 2006 to 2010, he was Research Associate with Liverpool Hope University, U.K., where he was associated with the Intelligent & Distributed Systems Laboratory. Since 2011, he has been with the Faculty of Computer Sciences & Engineering, GIK Institute of Engineering Sciences and Technology, Pakistan. He is currently working as Associate Professor and Director Huawei Authorised Information and Network Academy. He is a co-founding member of the Telecommunications and Networking (TeleCoN) Research Lab at GIK Institute. Dr. Abbas is a Fellow of the Institute of Science & Technology, U.K., a Fellow of the British Computer Society, and a Senior Member of the IEEE. His research interests include computer networks and wireless and mobile communications.

Frank Yong Li received the Ph.D. degree from the Department of Telematics, Norwegian University of Science and Technology, Trondheim, Norway. He was a Senior Researcher at UniKÃ¢Â€Â”University Graduate Center, University of Oslo, Oslo, Norway, before joining the Department of Information and Communication Technology, University of Agder, Grimstad, Norway, in August 2007, as an Associate Professor and then a Full Professor. Over the past few years, he has been an active participant in several Norwegian and EU research projects. He was listed as a Lead Scientist by the European Commission DG RTD Unit A.03Ã¢Â€Â”Evaluation and Monitoring of Programmes in November 2007. His research interests include medium access control mechanisms and routing protocols in fifth-generation mobile systems and wireless networks and the Internet of Things; mesh and ad hoc networks; wireless sensor networks; device-to-device communication; cooperative communication; cognitive radio networks; green wireless communications; reliability in wireless networks; quality of service, resource management, and traffic engineering in wired and wireless internet protocol-based networks; and analysis, simulation, and performance evaluation of communication protocols and networks.